APPENDIX A: Request for Additional Information Responses

REQUEST FOR ADDITIONAL INFORMATION

RELATED TO TOPICAL REPORT SSP-14/P01-028,

"GENERIC APPLICATION OF THE STUDSVIK SCANDPOWER CORE MANAGEMENT SYSTEM TO PRESSURIZED WATER REACTORS"

(CAC NO. MF7273)

1. **Please provide details regarding the range of applicability of various fuel designs, cladding types, burnable and other coated poisons, etc. that can be analyzed using the CMS5 code system:**

   a. **Range of Uranium enrichment in UO_2**
   b. **Types of claddings used in pressurized water reactors (PWRs) and their material compositions**
   c. **Nominal range of fuel pellet density as a fraction of the theoretical density of UO_2**
   d. **The range of enrichment of poison isotope in integral burnable absorbers types: Gadolinia (Gd_2O_3) and integral fuel burnable absorber (ZrB2 (For example the maximum Gd enrichment in Gd_2O_3])**
   e. **If coated pellet are used the maximum coating thickness that can be analyzed using the CMS5 code system.**
   f. **Fuel rod average burnups and peak pellet burnup (or range of burnups)**
   g. **Range of linear heat generation rate that can be handled by the CMS5 code system**
   h. **Maximum boron concentration in coolant that can be handled by CMS5**
   i. **Control Rod absorber types: B4C, Ag-In-Cd, W and Hafnium and the isotopic enrichment for the poison/absorber in the control rods**
   j. **Reflector materials, their compositions and dimensions**
   k. **Baffle materials, their compositions and dimensions**
   l. **Incore and excore detector types and absorber material(s) used in detectors**
   m. **Any other parameters or fuel designs.**

The CMS5 code system was not designed to limit the range of materials or conditions that could be modeled. The limitations are typically governed by the available data for benchmarking and uncertainties. The ranges of applicability of the parameters listed here are based on our analysis experience, expertise in nuclear data, and intimate knowledge of the code functionality.

a. To clarify, this item refers to the range of ^{235}U enrichment in UO_2: Natural to 10% ^{235}U. It is recognized that the USNRC currently cannot license the use above 5%. Studsvik Scandpower is willing to accept a limitation to 5% with recognition that the code system could model values higher than this. This would allow for flexibility if the current licensing maximum value is changed.

b. The table below for CASMO5 default compositions used for PWR cladding is taken from Section 3. The natural element weight percent is also listed in the table. The default stainless steel is listed on a

separate table below, although it is can be used as both cladding and structural material. In general, CASMO5 is capable of handling any cladding material. Typical clad materials are composed of Zr, Nb, Sn, Fe, Cr, Ni, O, which CASMO5 can model in any ratio. Cladding materials such as the TVEL E110 & E635 and Japanese NDA & MDA may also be defined as cladding compositions in CASMO5 (although default compositions are not internally provided by the code.)

CASMO5 also provides default compositions for materials typically used in structural components, such as spacer grids. The table below summarizes these compositions and the default elemental weight percent in CASMO5.

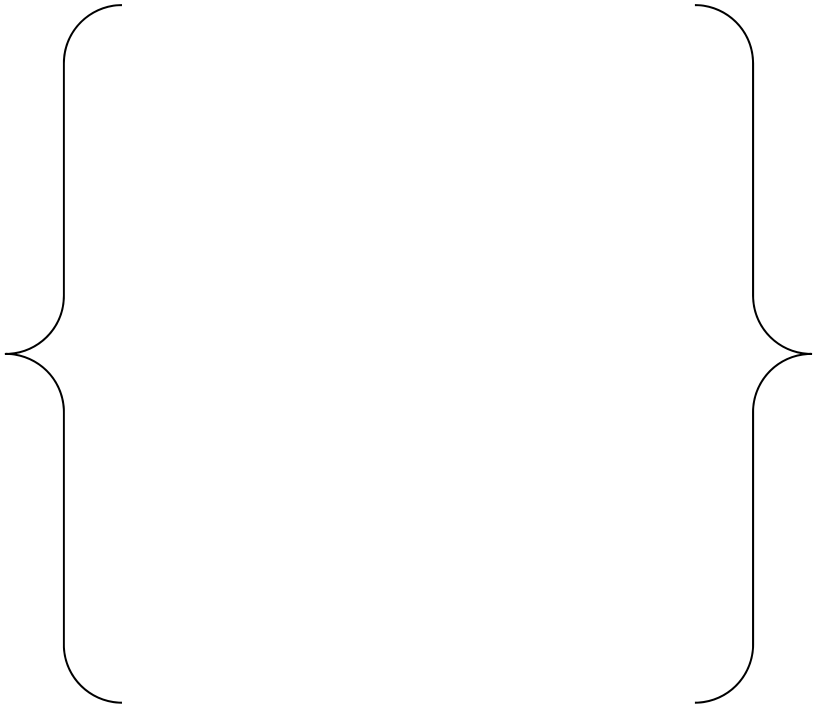

The values listed for the CASMO5 default material compositions are estimates to aid the user in the process of building core models. Due to the *proprietary* nature of several materials, the *exact* composition may differ from the default values. However, the user is free to enter the specific compositions if provided by the fuel vendor.

While CASMO5 offers a set of generic mixed zirconium, stainless steel, Inconel and other materials, we have not prescribed any material restrictions. The use case for our current users both internally and outside of Studsvik Scandpower is mixed. About half use the premixed Zircaloy compositions we provide, and the other half build the materials as a mixture within the code to the specification provided by the fuel vendor. In the TR we used the premixed Zircaloy materials, while performing a sensitivity analysis to those versus vendor specific compositions. The result of the sensitivity showed negligible difference in the computed eigenvalue or power distributions. We have also performed studies of some of the Accident Tolerant Fuel concepts including layered cladding designs. We have found very good performance of the CASMO5 code as compared to MCNP and SERPENT. Studsvik follows new initiatives and has extensive interaction with customers on this issue. In summary there is no mechanical limitation in the code system on the cladding materials. Through our QA process of individual code benchmarking and integral benchmarking, we have proper configuration management processes to model evolving fuel cladding designs.

c. The CASMO5 code requires the user to enter the calculated fuel pellet stack density, after accounting for porosity, dishing, chamfering, etc. at nominal (cold) conditions. The U-235 enrichment and burnable absorber weight percent will also impact the nominal fuel pellet density. For example, nominal densities may be as low as 9.5 g/cc for fuel pellets containing Gd_2O_3 in certain PWR assemblies. Conversely, some PWR fuel assemblies may involve relatively higher nominal density, up to 10.9 g/cc. The typical range for current operating PWR reactors is between 10.3 and 10.6 g/cc (or between 0.94 and 0.97 as a fraction of theoretical density). However, there are no formal limitations on fuel pellet densities in CASMO5, and therefore CMS5, outside this narrow range (beyond, of course, requiring non-zero, non-negative values).

d. CMS5 is capable of modeling enriched Gd, though typical gadolinia burnable absorbers use natural Gd. (There is some experience in the past with CASMO-4/SIMULATE-3. See K-H Bejmer, and O. Seveborn, "Enriched Gadolinium as Burnable Absorber for PWR," PHYSOR-2004, Chicago, IL, 2004.) Typical integral burnable absorber Gd_2O_3 may range up to 12% as a mass fraction of the total fuel weight. Limits on B-10 enrichment for IFBA ZrB_2 absorbers are better defined in terms of total pin B-10 linear load in mg/cm, as explained in the next item.

e. The CMS5 code allows the user to model coated pellets, such as IFBA, by specifying the total segment B-10 loading and effective coating layer thickness. The B-10 number density is subsequently computed based on these assumptions. Therefore, the user can specify a large (or small) thickness and the number densities are automatically adjusted to preserve the total B-10 atoms for IFBA over the assembly. Geometrically, the coating layer thickness $\Delta_c > 0$ must respect the following relation: $r_f + \Delta_c \leq r_{ci}$, where r_f is the fuel pellet outer radius and r_{ci} is the cladding inner radius.

f. The CMS5 system has been used for the benchmark models in the topical report to calculate the following burnup from a high burnup demonstration assembly:

- Peak average assembly burnup ≈ { } GWD/MT

- Peak average fuel rod burnup ≈ { } GWD/MT
- Peak pellet burnup ≈ { } GWD/MT

Separate from the topical report, another user has published isotopic comparisons and reactivity effects with burnup up to 120 GWD/MT (Ref 1 and 2).

1. Peter Grimm, Gregory Perret, Hakim Ferroukhi, "CASMO-4E and CASMO5 Analysis of the Isotopic Compositions of the LWR-PROTEUS PHASE II Burnt PWR UO2 Fuel Samples" PHYSOR 2014, Kyoto, Japan. Sept. 28-Oct. 3, 2014.
2. Peter Grimm, Gregory Perret, Hakim Ferroukhi, et. al., "CASMO5 Analysis of Reactivity Worths of Burnt PWR Fuel Samples Measured in the LWR-PROTEUS Phase II", PHYSOR 2016, Sun Valley, ID. May. 1-5, 2016.

g. The LHGR is not a fundamental physical property modeled by the CMS5 system. LHGR values result from selections of core geometry and total core power. The CMS5 code system is limited by heat transfer modeling capabilities of SIMULATE5. The TH models in SIMULATE5 can perform up to the onset of DNB. Thus we limit any analysis in SIMULATE5 to conditions below this point.

h. CASMO5 is capable of generating cross section for downstream SIMULATE5 analysis spanning a range of boron concentrations. The automated S5C case matrix in CASMO5 will vary the boron concentration to cover normal power operation and also shutdown boron concentrations, and can easily model beyond 3000 ppm, though this is not a limit. The practical limits are below the solubility limit as we do not model precipitation of the boric acid.

i. In CASMO5 and therefore CMS5 there are no formal limitations on the isotopic enrichment used when defining control rod absorber materials. To aid the user, CASMO5 provides default material compositions for { }. The default values for the isotopic weight percent for these materials, which are provided in the CASMO5 User manual (Section 2.3), are based on the average natural abundance.

j. Typical PWR reflector materials involve light water, air, stainless steel, zirconium and Inconel. The compositions of the latter three are listed under item b) above. In both the axial and radial dimension some modeling approximation must be applied to generate cross section data for the reflector nodes using a two-dimensional code, such as CASMO5. The reflector material in the axial (top and bottom) regions is volume-homogenized into several compositions using the HOx option in CASMO5. Proper volume fractions must be calculated outside CASMO5 and directly entered into the input file. Conversely, the relative simplicity of the geometry in the radial dimension enables the user to forgo volume homogenization, although the physical baffle and barrel geometry must still be approximated as slabs. A very simple schematic of the “equivalent” CASMO5 reflector model and the “actual” core geometry is depicted in the schematic below.

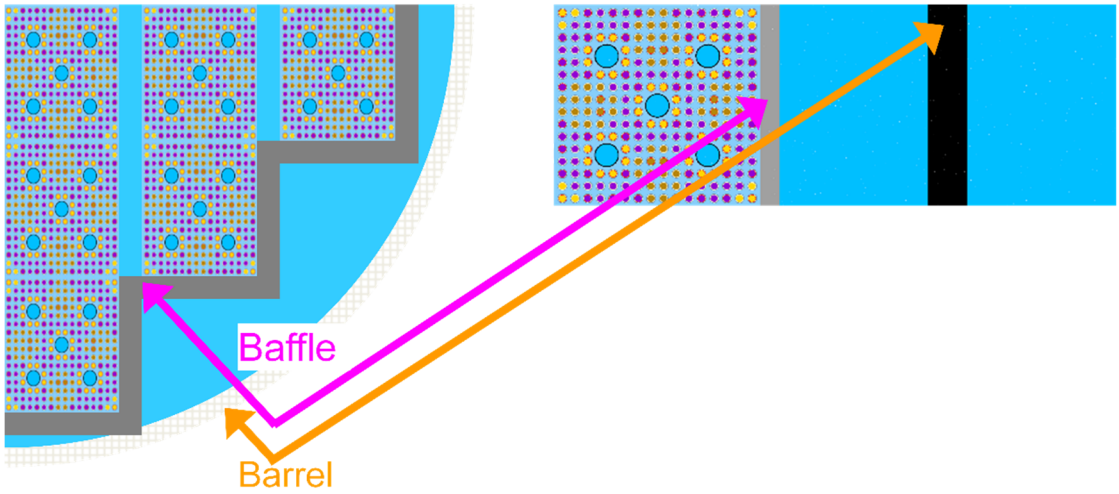

The purpose of the reflector calculations is to calculate appropriate discontinuity factors at the boundary of the core. To ensure these are properly converged it is recommended that the thickness be at least { } cm. At this thickness the flux is near zero at the exterior boundary as it would be in the reactor. At thicknesses greater than { }cm the discontinuity factors may begin to diverge due to the solution technique used in fitting the flux shape to calculate the discontinuity factors. Our training provided to the customer emphasizes this point, and we recommend that users build appropriate understanding by performing a sensitivity analysis.

For the remainder of the CMS5 system the reflector regions are treated as segments and processed in CMSLINK5 and then assigned in SIMULATE5 to the proper location either surrounding the core as a radial reflector, or on the top and bottom of the fuel as top or bottom reflectors. For PWR calculations the radial reflector can use the submesh calculations for more detailed predictions of the flux gradients at the core boundary.

k. In practice the baffle region is always part of the radial reflector. The baffle becomes a region in the radial reflector problem and no limitations apply from a computational standpoint other than those discussed in Item J.

l. CMS5 is capable of modeling incore detectors as part of the cross section generation procedure. Typical PWR incore detectors involve the presence of an instrumentation tube in the fuel assembly with a thimble. Typical detector types include movable U-235 fission chambers and self-powered neutron detectors (SPND) with the following materials: { } Other movable and SPND detector types can also be modeled in CASMO5 by specifying the nuclide identification and reaction type.

CMS5 is also capable of modeling excore detector response at the core simulator level using SIMULATE5. The source range and power range excore detectors can be modeled. The source range excore detector calculations are typically coupled with the fixed-source calculations in which the reactor is sub-critical and the flux distribution inside the core is determined by the distribution of internal and external neutron sources. The excore detector model is a relative response model and does not model the physical detector absorber material.

m. There are no other limitations that are considered for the CMS5 system beyond what has been discussed in the previous items.

2. **Explain summary details of how the CMS5 code system works interactively, in terms of processes such as the migration and maintenance (propagation) of uncertainty in neutronics parameters from one code to the next during the coupling process. Please provide a flow chart of CMS5 code system similar to one that was shown during the audit.**

The CMS5 code system works as a three-part system.

1. The CASMO5 2D lattice physics code is run for each unique 2D composition of a fuel assembly, referred to as a segment. The segment is run at a base condition and various perturbations to calculate the entire operational conditions that it may see during reactor life and storage conditions. The data needed by the other two parts of the system is stored on a card image file.
2. The CMSLINK5 linking code is run for each card image file, i.e., for each segment, that was calculated in CASMO5. The purpose of CMSLINK5 is to take the data needed from the card image file to create cross-section tables for use in the core simulator SIMULATE5.
3. The SIMULATE5 core simulator code is used to simulate the operation of the reactor in 3D. The results of these simulations are used to compare to operating reactor measurements for the purpose of uncertainty generation. This is also where calculation results are produced to provide operational guidance, core monitoring input data, and inputs to the safety analysis.

In summary the uncertainties are all determined at the core simulator level in SIMUALTE5 for the application under review. Here all of the model and measurement uncertainty for the CMS5 system are lumped into the total uncertainty. No attempt is made to separate or propagate error components. This is done in the interest of time and consistency with current core physics code licensing methods.

Below is a flow chart showing how information is input into and propagated through the CMS5 system. The process concludes by comparing measurements to predictions, which are used to determine uncertainties.

Figure 1: CMS5 Flowchart

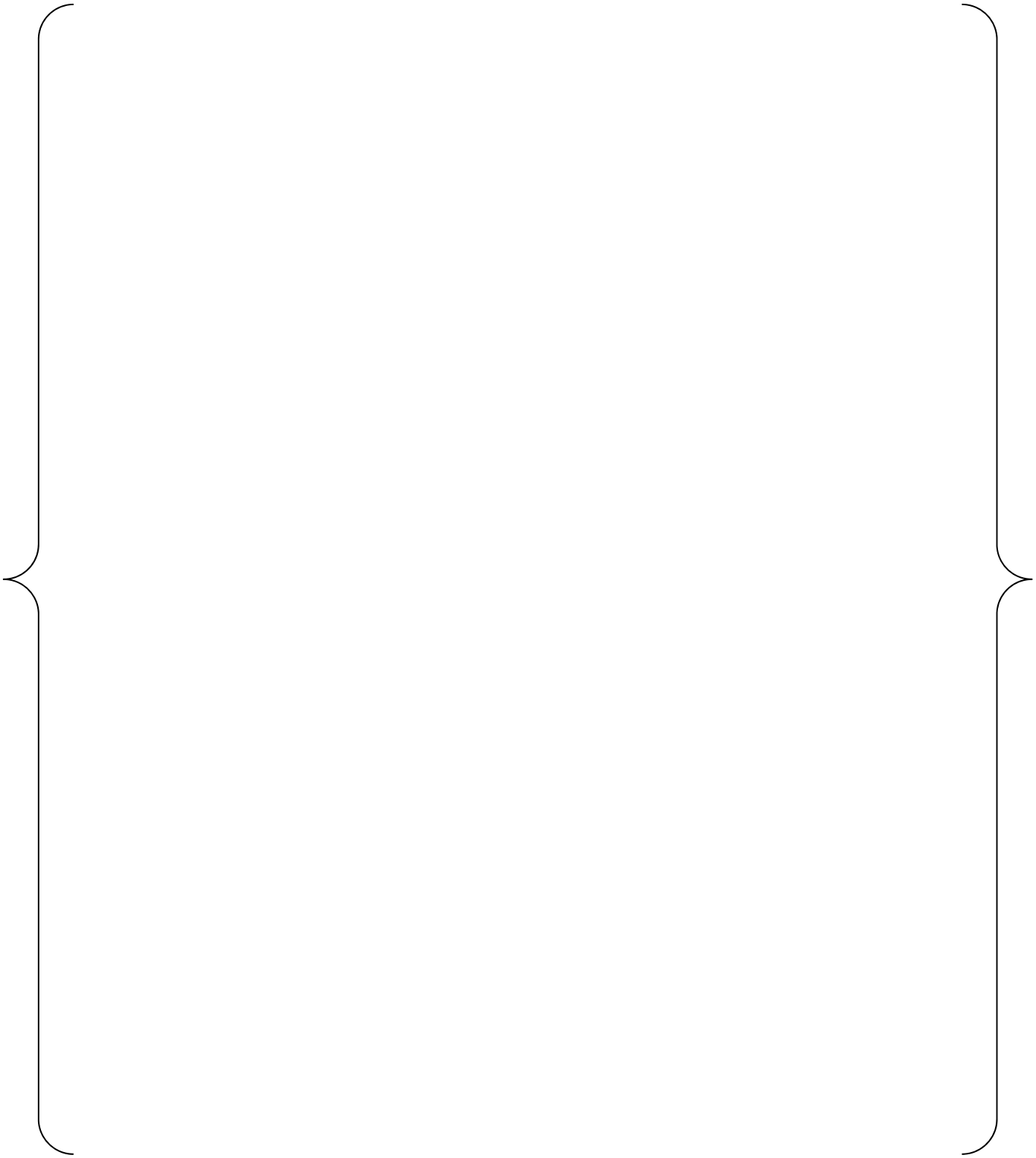

3. Section 5.3.1 of the SIMULATE5 methodology document briefly describes the geometry used in the depletion model. Figure 5-1 provides the axial nodalization of an assembly in the depletion model without providing any nodal dimensions. What is the impact on sensitivity and accuracy of the depletion results for different model dimensions?

SIMULATE5 employs a "subnode" concept in which the fuel assembly is axially divided into materially homogeneous "subregions". Fig 5-1 is a simple demonstration of the axial geometry used. The number of axial nodes doesn't represent the actual modeling. The subnodalization is used both with the axial homogenization and depletion models.

The difference between the axial homogenization model subnodalization and depletion model subnodalization is that the material discontinuity due to control rods is ignored in the latter case. The depletion subnodes are defined as the combination of the following:

- User defined axially uniform mesh
- Enrichment/Burnable Absorber zoning
- Fuel/Reflector zoning
- Spacers.

The user defines the number of axially uniform fuel nodes in a model. All axially uniform nodes have the same height (equal to the core height divided by the number of nodes). Typically, { } to { } axial nodes are used with PWR models. If there is any material heterogeneity within boundaries of an axially uniform node, SIMULATE5 further divides the axial node into smaller subnodes which are materially homogenous. Thus, the maximum axial node height used with the depletion model is never more than { } cm when a typical PWR model is run with { } axial nodes (or around { } cm with { } axial node model). It is important to note that the depletion subnodalization may differ from one fuel design to another.

Burnup, history parameters and nuclide data are stored subnode-wise in SIMULATE5. Thus the ambiguity with keeping track of the same distributions in conventional "materially-heterogeneous" nodes is avoided. Moreover, the subnode power/flux used with incrementing depletion arguments is obtained from the solution of the 1-D multi-group diffusion equation, which explicitly accounts for each heterogeneity. Thus the flux solution is insensitive to the number of uniform axial nodes.

An example calculation has been performed for a 7 cycle PWR model. This calculation was performed once with { } axials nodes and a second time with { } axial nodes. Following each cycle, a comparison is made with the top and bottom { } cm regions (where the largest axial flux gradient is typically found) where the resulting exposure was found to be less than { } GWD/MT, or about { }%). The figure below compares the axial burnup distribution for an assembly with maximum end of life burnup. For this fuel assembly, the { } node model internally tracks the burnup in { } depletion subnodes whereas the { } node model uses { } depletion subnodes. The { } node model captures all the details, including spacer/grid suppressions, in the assembly burnup distribution.

An additional sensitivity was performed using a benchmark model from the topical report, Plant D Unit 2. The following table presents the differences in selected core attributes for a SIMULATE5 depletion run with two different axial node selections, changing from { } nodes to { } nodes. As can be seen from the table results, the model is relatively insensitive to the { } cm change in node height when the number of axial nodes is reduced from { }.

Change in Selected Core Parameters When Using { } Versus { } Axial Nodes

(Plant "D", Unit 2, Cycle 20)

Exposure GWD/MTU	Power %	Change In Critical Boron (ppm)	Change In Core Maximum 4PIN (Fq)	Change In Core Maximum 2PIN (FdH)	Change In Core Axial Offset
0	0	0	0.005	0.001	0.001
0	100	0	-0.001	0	0
0.15	100	0	0.003	0	0
0.5	100	0	0.004	0.001	0
1	100	0	0.002	-0.001	0
2	100	1	0.001	0.001	0
3	100	0	0.002	-0.001	0.001
4	100	1	0	0	0
5	100	0	0.001	0	0.001
6	100	1	0.001	0	0
7	100	0	0.001	0.001	0.001
8	100	1	0.001	0	0.001
9	100	1	0	0	0.001
10	100	0	-0.002	0	0.001
11	100	0	-0.001	0	0
12	100	0	0	0	0
13	100	1	0.001	0	0
14	100	0	0.002	0.001	0
15	100	1	0.003	0	0
16	100	1	0.002	0	0
17	100	0	0.002	0	0
18	100	0	0.002	0	0.001
18.5	100	0	0.002	0	0.001
19	100	0	0.001	0	0
19.249	100	1	0.001	0	0

4. SSP-14-P01/012-R, Revision 1 states that the effective cross sections are used in a series of 1D, collision probability micro-group calculations to obtain detailed neutron energy spectra for use in the condensation of the cross sections. The following questions are related to the cross section processing in CASMO5.

(a) Section 2.3.3 states that in order to decrease execution time, the cross sections are condensed with an approximate flux spectrum. Explain how the energy condensation of the cross section is done. Also, explain whether or not the accuracy in the results is compromised due to condensation of cross sections.

(b) Explain how the cross sections developed in the above process (1-D) are compatible with the CASMO5 2-D transport theory code and eventually compatible with the SIMULATE 5 multi-group diffusion or simplified P3 transport equation solutions.

(c) Section 2.3.3 of the CASMO5 Methods and Validation Report states that accurate collision probabilities for the cylindrical pin cell with flat source in each region are calculated using the FLURIG-2 method developed by Carlvik. Please provide details regarding this FLURIG-2 method.

(d) Please explain (in more detail than provided in CASMO5 Methodology Manual) the resonance upscatter model included in CASMO5. What is the impact of the resonance upscatter model on the Doppler temperature coefficient (DTC) in CMS5 code system?

(a) The energy condensation scheme in CASMO5 consists of 1D pin cell calculations performed before the 2D lattice calculation. The pin cell calculations are performed in the micro-group structure of the neutron cross section library (586 groups). The flux solution from the 1D pin cell calculations, which is also in the micro-group structure, is used to condense the macroscopic cross sections to the 2D-group structure.

A micro-group calculation is performed for each pin type in the fuel assembly. Spectral effects are modeled in the micro-group calculation to preserve the accuracy of the energy condensation. Normal fuel pins are modeled using either three or four regions (*e.g.*, fuel, air, cladding and coolant). If the lattice being modeled contains water gaps outside the fuel assembly, an additional region representing the water gap is added to the cell. This region creates the "softening" effect which the bypass region (typically in BWRs) has on the flux distribution across the cell. For inert rods (*e.g.*, water rods, guide tubes, etc.), a fuel-containing "buffer" region is added to the outside of the coolant and is used to drive the flux across the cell. Burnable absorber rods are modeled using a geometry similar to that used for inert rods.

The accuracy of the results is discussed in the response to part (b) below.

(b) The 1D micro-group calculation involves a detailed representation of each pin type in terms of energy and local spatial effects. The resulting micro-group flux, which captures *local* spectral effects, is used to condense cross sections that are unique to the specific pin type. Therefore, *local* spectral effects are conserved by the micro-group calculation by condensing cross sections to the appropriate 2D-group data for each pin type in the assembly. The 2D transport calculation uses the 2D-group cross sections to obtain the neutron flux solution over the entire assembly, thereby providing all the data necessary for SIMULATE5, since quantities such as Discontinuity Factors (DFs) cannot be obtained from 1D pin cell calculations in an accurate and straightforward manner.

The generation of the SIMULATE5 sub-mesh data is tallied during the 2D transport calculation. The neutron flux from the transport calculation is spatially homogenized over pre-defined sub-mesh regions and the 2D-group data is condensed to the few-group SIMULATE5 energy structure, which is 8 groups by default. The energy condensation is performed in the same manner as the condensation of the micro-group structure to the 2D-group structure. The sub-mesh data includes the neutron flux, surface net currents, cross sections, diffusion coefficients, and fission spectrum. In addition to sub-mesh data, the assembly-averaged data for analogous quantities are also edited by CASMO5 after the 2D transport calculation.

Since the Simplified P3 (SP3) option in SIMULATE5 only involves the solution of an additional equation, referred to as the P3 equation, in addition to the standard P1 equation, no additional data is necessary from CASMO5 when using the SP3 option in SIMULATE5.

(c) The FLURIG-2 method is an approach to computing collision probabilities in one-dimensional cylindrical geometry which improves the numerical evaluation of the integrals expression by removing singularities through a change of variables. Since the evaluation of the integral is performed using a Gaussian quadrature (Abramowitz and Stegun, p. 921), the presence of a singularity in the integrand function would render the quadrature approach unsuitable. The FLURIG-2 method is simply a numerical technique and does not change the theory behind the collision probability method.

(d) The resonance upscatter (RUP) model in CASMO5 is essentially a set of correction factors that are applied to the { } (and { }) resonance absorption integrals (RIs).

The RUP model is motivated by the fact that standard cross section processing codes, such as the NJOY GROUPR module, assume an asymptotic scattering kernel to model neutron-nucleus elastic scattering interactions in the epithermal range. The flux spectrum calculated under the asymptotic assumption results in multi-group data which underestimate the upscatter effects near scatter resonances. Physically, the asymptotic scattering kernel assumes that the target nucleus is at rest. In order to correct the deficiency, the RUP factors must be generated using a Monte Carlo Slowing Down (MCSD) code, which is capable of calculating accurate RIs using the asymptotic and *exact* scattering kernels. The choice of Monte Carlo simulation greatly simplifies the implementation and circumvents the mathematical complexity of solving the *exact* scattering kernel (which explains why the *exact* kernel is not present in conventional cross section processing codes.) Once the RUP factors are obtained, they are applied to the RIs as described in CASMO5 Methods and Validation Report.

The effect of the RUP model at the CASMO5 lattice level can be understood by comparing predicted k-infinity and temperature coefficient. In particular, the UO_2 Doppler benchmark proposed by Mosteller (R.D. Mosteller, "ENDF/B-V, ENDF/B-VI, and ENDF/B-VII.0 Results for the Doppler-defect Benchmark," M&C+SNA 2007, Monterey, CA., 2007) has been analyzed and results summarized in the table below for CASMO5 v2.06.00 and the e7r1.202.586.bin library.

Enrichment (w/o)	k (Asymptotic kernel)			k (Exact kernel)			FTC Diff. (%)
	HZP	HFP	FTC	HZP	HFP	FTC	
0.711							
1.6							
2.4							
3.1							
3.9							
4.5							
5.0							

The results indicate that the exact scattering kernel, obtained by applying the RUP factors to RIs, { } the Fuel Temperature Coefficient (FTC) by an average of { }%. { } absorption is predicted by the exact kernel, resulting in a { } of the k-infinity at Hot Full Power (HFP) and Hot Zero Power (HZP). However, the { } in absorption is { } in HFP relative to HZP, and therefore the FTC is { } when the RUP model is active and the exact kernel is used. The figure shown below depicts the FTC values tabulated in the table above.

{The current version of CASMO5 undergoing licensing does not make use of the RUP model by default, although the RUP model is still available as an option.}

5. The following questions are related to the SIMULATE5 methodology for cross section processing and depletion models: (Please answer the questions below in more detail than what was in the draft responses provided during the audit)

a) It has been stated that SIMULATE5 uses "quadratic Gd depletion model" from CASMO5. Please explain the details of how the quadratic depletion model is implemented in CASMO5 and SIMULATE5.

b) Explain the "hybrid macroscopic/microscopic depletion" model that is used in SIMULATE5.

c) It is stated that radial submesh cross-sections and discontinuity factors are less dependent on the CASMO boundary conditions (BCs) than the full assembly counter parts. Why is this? Does this hold true for edge meshes that are a single pin cell thick? What about corner meshes that are only comprised of a single pin cell and are bordered by two BCs?

a) The Quadratic Gd depletion model implemented in CASMO5 and SIMULATE5 solves the burnup equations for Gd chains (Gd-152 through Gd-161 in CASMO5 and the simplified Gd-154 to Gd-155 to Gd-156 to Gd-157 chain in SIMULATE5). The model assumes that the microscopic absorption reaction rates of gadolinium isotopes are quadratic functions of the number density of Gd-155. This quadratic function models the variations of the spatial shielding effects over the depletion step and therefore improves the overall accuracy of depletion calculations.

The burnup equation for isotope *m* is:

$$\frac{dN_m(t)}{dt} = N(t)_{m-1}\sigma_{m-1}(t)\phi(t) - N(t)_m\sigma_m(t)\phi(t) \qquad \text{Eq. 1}$$

where N_m is the number density of isotope *m* as a function of time *t*, $\sigma_m(t)$ is the microscopic capture cross-section and $\phi(t)$ is the neutron flux. The quadratic expansion differs from the the conventional predictor/corrector depletion method, in which the absorption rate $\sigma_m(t)\phi(t)$ is assumed to be constant during each step.

The quadratic assumption can be written as:

{ } Eq. 2

where { }is the { } per atom of isotope { }; { }are coefficients of the quadratic function; { } and m={ } and { }. Three coefficients for each gadolinium isotope are determined using three sets of { }.

For the corrector step from t_n to t_{n+1} (where n is the depletion step number), this set is known at t_{n-1}, t_n and t_{n+1}. For t_{n+1}, the predictor information from a conventional predictor/corrector method is used; *i.e.,* the quadratic depletion method is applied to the corrector step only.

Once the coefficients are determined, Eq. 1 is integrated using a sub-step integration method (time step t_n to t_{n+1} is divided into smaller time steps), in which the value of {R_m }is computed using Eq. 2 for each sub-step.

In the predictor/corrector depletion as well as quadratic depletion, only one flux calculation (using the predictor step number densities) is performed per statepoint to save calculation time. Even though the corrector step number densities are accurate, the flux and eigenvalue solution may not be as accurate as the corrector number densities. To overcome this deficiency, the predictor number densities are {post corrected} as shown below:

{ } Eq. 3

where the { } is defined as

{ } Eq. 4

where subscripts *m, n* are indexes for isotope and time step, superscripts *p, c, u* stand for predictor, corrector, and { }. This { } is based on the approximation that the { } in the number density { } is { } over the depletion. After the post correction, the flux calculation is performed with the corrected predictor step number density{ }.

One key assumption with the quadratic Gd depletion model is that the reaction rates { } with depletion, meaning it is well suited for a constant depletion (without step changes in power or control rod insertion/withdrawal, for example) as is typically performed in a lattice code or for PWRs in a nodal code.

The quadratic Gd depletion model is { } in SIMULATE5. The { } is an effective Gd model with sub-step integration as described in the methods manual (see Section 5.3.3). Within this model the chain of gadolinium isotopes (Gd-155 to Gd-156 to Gd-157) is replaced by an effective Gd isotope (W. Weiss, “A Consistent Definition of the Number Density of Pseudo-

Isotopes," Ann. Nucl. Energy, Vol 17, No.3, pp 153-156, (1990)). The number density and microscopic absorption cross section for the effective Gd isotope are defined as:

Eq. 5

Eq. 6

The effective isotope preserves the absorption reaction rates of the isotope chain. The microscopic absorption cross section of Gd^{eff} is given as a function of the number density of Gd^{eff} itself. The advantage of using the effective Gd isotope over individual Gd isotopes is that the change of absorption cross section as a function of the number density becomes much less pronounced. This enables larger depletion steps for integrating the effective chain. { } is improved for the effective Gd depletion model in SIMULATE5 by use of substep integration, where each depletion step is divided into substeps (with a typical substep size of { } MWD/kg). The effective absorption cross section is recomputed at the end of each substep using the most recent number density of Gd^{eff}.

b) The hybrid macro/micro cross-section/depletion model implemented in SIMULATE5 computes the node-average cross sections for the given actual condition as:

Eq. 1

where { }represents { } and where the summation is over selected nuclides.

The first two terms represent the *macroscopic depletion* model with the single assembly cross sections which are generated from CASMO5 and tabulated as functions of exposure and instantaneous (such as fuel temperature, coolant density, control rod) and history (such as coolant density history, boron history, control rod history) state variables. The values of the nodal history variables are computed by { }. For instance, in depleting a node from exposure E_n to $E_n + \Delta E$, the history value, HV, for parameter V (V could be moderator temperature, boron concentration, void, etc.), is computed by the equation:

Eq. 2

where w is a history weighting parameter with a typical value around { }. The weighting is larger than { } to account for the fact that the cross sections are { } to the { } values of the state parameters, and { } to those from the distant past. SIMULATE5

automatically computes one value of the weight function for each fuel type by using data from the history depletions that are available in the cross-section library.

The third term in Eq. 1 provides a correction to the single-assembly macroscopic cross sections (Σ^{SA}) to compensate for the fact that actual operation (represented by number density N^{actual}) differs from the idealized condition modeled by the single assembly CASMO5 evaluation (represented by N^{SA}).

For the microscopic cross sections, approximately { } isotopes ({ } actinides, { } fission products, Gd and B^{10} as burnable absorber) have been chosen according to their importance for reactivity during normal operation, depletion, transients, and shutdowns (with possible long outages).

Both the macroscopic and microscopic multi-group cross sections appearing in Eq. 1 are functionalized into two-, three- or four-dimensional tables as a function of all important instantaneous effects (*e.g.*, coolant density, control rod presence, and fuel temperature) and historical effects (*e.g.*, burnup, coolant density history, and control rod history).

The reference single-assembly number densities are functions of burnup and historical effects. The N^{SA} are not taken directly from CASMO5 but calculated in the linking code (CMSLINK5) by solving the SIMULATE5 isotope chains using the single-assembly fluxes and microscopic cross sections. Hence, N^{SA} and N^{actual} are computed in a consistent manner.

For cross-sections other than macroscopic absorption and fission/nu-fission cross-sections, there is no microscopic depletion model correction. Therefore, they are purely represented by the macroscopic cross-section model as shown in Eq. 3 below:

{ } Eq. 3.

c) In traditional nodal methods, the node homogenized cross-sections and discountinuity factors are generated from a transport calculation for a fuel assembly in an infinite lattice environment. This assumption uses an idealized intra-assembly flux shape as a weighting function to collapse cross-sections. This intra-assembly flux shape will be different if the assembly is subjected to a different boundary condition. The variations in intra-assembly flux shape are encountered in PWRs where the fuel assembly is heterogeneous by design (*i.e.*, fuel assembly designs with asymmetric burnable absorber loadings typically used in initial cycles) or the intra-assembly heterogeneities introduced in any assembly that accumulates significant exposure with a skewed flux distribution (such as an assembly loaded on the core periphery where the flux gradient is steep).

SIMULATE5's radial-submesh model accounts for these deviations from the inifinite lattice boundary conditions and their impact on the assembly homogenized cross-sections.

The radial-submesh model divides the assembly into NxN subregions, where each submesh has its own homogenized cross-sections and discontinuity factors. The submesh homogenized cross-sections and discontinuity factors are generated from single assembly CASMO5 calculations along with their assembly homogenized counterparts. The default submesh layout has more radial resolution on the edges of the assembly than the interiors, which allows for a better approximation of the flux gradient between dissimiliar assemblies. The two outermost sub-meshes are one pin-cell thick, as depicted for a southeast quarter assembly in the Figure 1 below.

Figure 1: SE quarter assembly submesh for a 17x17 lattice

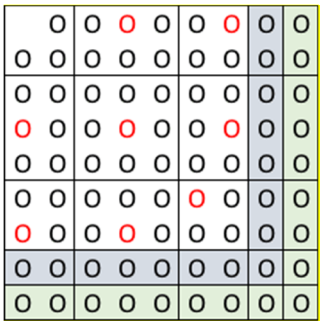

The submesh regions on the edges and corners of an assembly typically contain fuel pin(s) of a single fuel type. The corner regions contain just *one* fuel pin, making them more homogeneous than the full assembly. The resulting homogenized node constants and importantly the cross sections become less dependent on the flux shape used to collapse the cross sections. This reduces the error for the periphery and corner cells even while using the infinite-lattice flux shape in CASMO5.

To further elaborate, a detailed background discussion and example is presented below.

In SIMULATE5, the 2D diffusion equation is solved in the submesh geometry, one axial plane at a time. The resulting flux solution, which accounts for the true boundary condition of each assembly, is then used to weight the submesh cross-sections to compute the correct homogenized cross sections and radial discontinuity factors for the conventional 3D nodes.

A simple test case is presented here to demonstrate that the submesh cross sections are less sensitive to the single-assembly transport calculation boundary condition than their assembly-average counterparts.

The test case is a 4x4 assembly mini-core geometry (using quarter-core symmetry) containing a single fuel assembly design. The fuel assembly is strongy heterogeneous in the radial direction due to the placement of the burnable absorber rods in one of the quadrants of the fuel assembly. The assembly containing 8 Pyrex rods is depicted in Figure 2 below.

Figure 2: Asymmetric Assembly with Pyrex

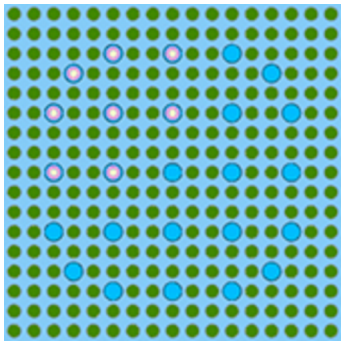

Two different 4x4 mini-core configurations are created, both constructed using the same fuel assembly, but with different assembly rotations. Core 1 has the Pyrex rods turned toward each other, whereas Core 2 has the Pyrex rods turned away from each other. The quarter core geometry of both cores are shown in the Figure 3 below.

Figure 3: Mini-Core Configurations with Pyrex

Core 1 Geometry (Quarter Core) Core 2 Geometry (Quarter Core)

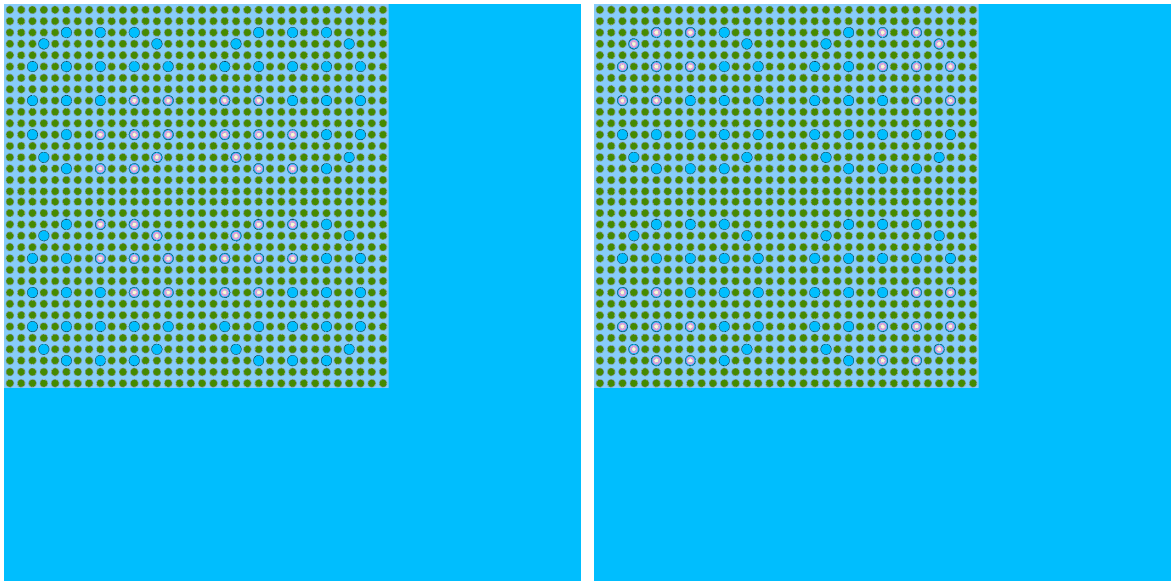

For the sensitivity study, cross-section libraries for SIMULATE5 are generated from single-assembly CASMO5 calculations using two different boundary conditions:

1) a single-assembly calculation with MIRROR bounday condition, which is equivalent to a *zero* net-current boundary condition,

2) a single-assembly calculation with PERIODIC boundary condition, which, due to the asymmetry of the assembly, corresponds to a *non-zero* net-current boundary condition.

Reference solutions for each mini-core are obtained from multi-assembly CASMO5 calculations. For each mini-core configuration, a set of SIMULATE5 calculations, each with 1 radial node per assembly nodalization, are run:

(i) Submesh Model OFF, Single assembly library data generated with MIRROR BC,

(ii) Submesh Model OFF, Single assembly library data generated with PERIODIC BC,

(iii) Submesh Model ON, Single assembly library data generated with MIRROR BC,

(iv) Submesh Model ON, Single assembly library data generated with PERIODIC BC.

This mini-core configuration, containing asymmetric fuel assemblies and surrounded by water reflector, exhibits strong flux tilt across the core, well beyond what is seen in a typical PWR core. The intra-assembly flux shape in each assembly significantly differs from the idealized flux shape used with the single-assembly CASMO5 lattice calculations. This severely limits the accuracy of the underlying infinite-lattice assumption used in the generation of the homogenized cross sections.

The eigenvalue and assembly power results are listed in Table 1 and 2 below.

Table 1 SIMULATE5 vs. Multi-Assembly CASMO5, Eigenvalue Comparisons for mini-core containing asymmetric assembly design with PYREX

Core	CASMO5 (Reference Eigenvalue)	SIMULATE5 Eigenvalue (pcm error from reference)			
		Submesh OFF		Submesh ON	
		MIR BC	PER	MIR	PER
Core 1	{ }	{ }	{ }	{ }	{ }
Core 2	{ }	{ }	{ }	{ }	{ }

Table 2 SIMULATE5 vs. Multi-Assembly CASMO5, assembly power comparisons for mini-core containing asymmetric assembly design with PYREX

Core	CASMO5 (Reference Assembly Powers - RPF)	SIMULATE5 (Relative Power Fraction (RPF) RMS Error %) Assembly RPF error (%)			
		Submesh OFF		Submesh ON	
		MIR	PER	MIR	PER
Core 1	{ }	{ }	{ }	{ }	{ }
Core 2	{ }	{ }	{ }	{ }	{ }

From Table 1 it can be seen that when the submesh model is OFF, the SIMULATE5 predicted eigenvalue is quite sensitive to the boundary condition used with the single-assembly CASMO5 calculations to generate the cross-section library. To highlight this, switching from MIRROR to PERIODIC bounday condition changes the SIMULATE5 error from { } pcm to { } pcm ({ } pcm delta) for core 1 and from { } pcm to { } pcm ({ } pcm delta) for core 2. Similarly, using the same library, the eigenvalue error changes significantly with core configuration (from { } pcm, core 1 to { } pcm, core 2 using MIRROR BC). When the submesh model is enabled, the variation in SIMULATE5 eigenvalue error is only { } pcm to { } pcm (with { } pcm delta) among all four cases, demonstating that the submesh model cross-sections are insensitive to the boundary condition employed and core configuration. The assembly power errors presented in Table 2 further confirm that the submesh model consistently provides better assembly power predictions for such heterogeneous core configurations where each assembly is subject to different boundary conditions.

The same test is repeated using a different assembly design containing IFBA burnable absorbers. The IFBA pins on the edge row of the asymmetric quadrant have an alternating pattern (IFBA, No IFBA, IFBA, ...) as shown in Figure 4 below:

Figure 4: Asymmetric Assembly with IFBA

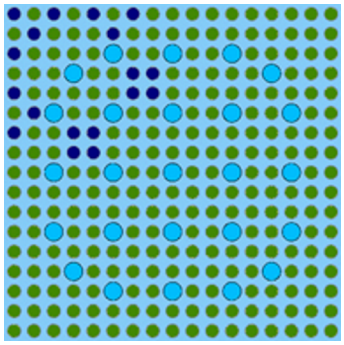

Two core configurations, differing in fuel assembly rotations, are run both with multi-assembly CASMO5 and SIMULATE5 in the geometry shown in Figure 5 below:

Figure 5: Mini-Core Configurations with IFBA

Core 3 Geometry (Quarter Core) Core 4 Geometry (Quarter Core)

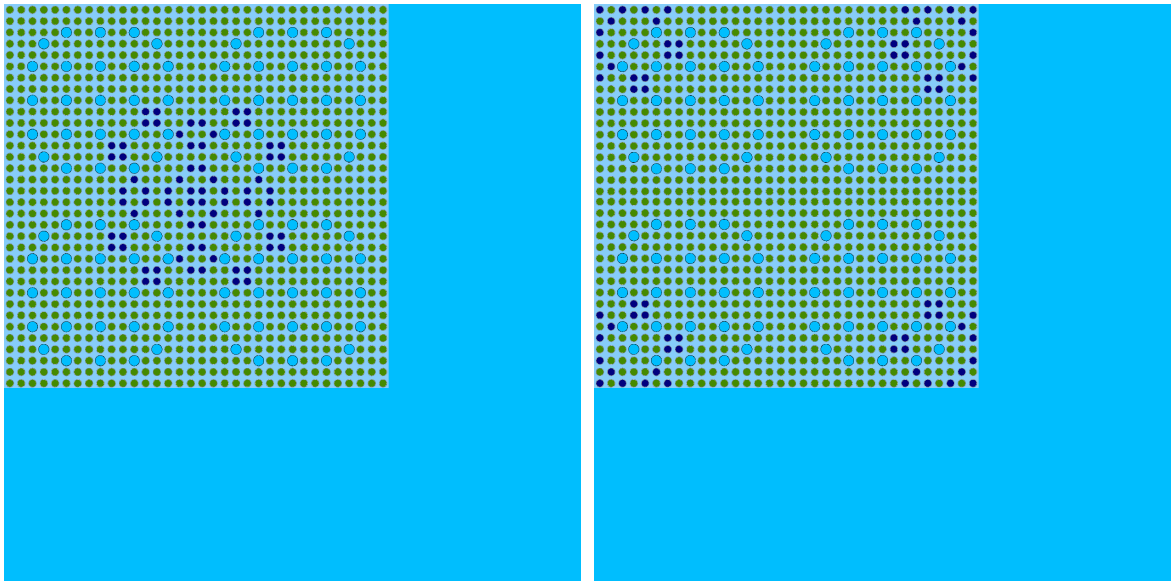

Eigenvalue and power comparions are presented in Tables 3 and 4 below.

Table 3. SIMULATE5 vs. Multi-Assembly CASMO5, Eigenvalue Comparisons for mini-core containing asymmetric assembly design with IFBA

Core	CASMO5 (reference Eigenvalue)	SIMULATE5 Eigenvalue (pcm error from reference)			
		Submesh OFF		Submesh ON	
		MIR	PER	MIR	PER
Core 3	{ }	{ }	{ }	{ }	{ }
Core 4	{ }	{ }	{ }	{ }	{ }

Table 4. SIMULATE5 vs. Multi-Assembly CASMO5, Assembly power comparisons for mini-core containing asymmetric assembly design with IFBA

Core	CASMO5 (Reference Assembly Powers - RPF)	SIMULATE5 (Relative Power Fraction (RPF) RMS Error %) Assembly RPF error (%)			
		Submesh OFF		Submesh ON	
		MIR	PER	MIR	PER
Core 3	{ }	{ }	{ }	{ }	{ }
Core 4	{ }	{ }	{ }	{ }	{ }

As in the previous case (with Pyrex), SIMULATE5 results with the submesh model active are quite insensitive to the boundary condition used with the single-assembly CASMO5 calculations, even for assembly designs with edge fuel pins that neighbor dissimilar pins.

As a final note, the submesh model also tracks important actinides to capture the intra-assembly burnup shape. The choice of one-pincell thick outer regions, where the burnup gradient of an assembly is largest, captures the heterogeneity introduced due to depleting the fuel assembly with a flux shape

different than those used with single-assembly calculations in CASMO5. This further improves the accuracy of the depletion of the assembly within the core.

6. The following questions are related to the SIMULATE5 fuel temperature measurement validation using HALDEN rods that is used in the SIMULATE5 thermal-hydraulic model.

a) Provide a list of the HALDEN rods that have been used in the fuel temperature validation listing the end of life (EOL) burnup and Gadolinium content, if any.

b) An outstanding issue related to the thermal-hydraulic-mechanical and material design of UO_2 fuel is the thermal conductivity of irradiated UO_2 fuel considering the effects of burnup (exposure). The thermal conductivity of irradiated UO_2 fuel is affected by changes that take place in the fuel during irradiation, such as solid fission product buildup (both in solution and as precipitates), porosity, and fission gas-bubble formation.

The fuel thermal conductivity section of SIMULATE5 (Section 10.3.1) describes the UO_2 and MOX thermal conductivity with a correction factor (r_p) for fuel density to account for the effect of fuel burnup on thermal conductivity.

Provide details regarding the basis and formulation of this factor that appears in Equations 10.3.4 and 10.3.5) of the SIMULATE5 Methodology manual. Is this factor related to the HALDEN rod data mentioned in (a) above?

a) The table below provides the relevant data of the fuel rods from the Halden experimental program that have been used for the validation of the SIMULATE5 fuel pin model [1,2]. None of the fuel rods contain gadolinium.

Rod #	Gap (mm)	Pellet OD (mm)	Pellet ID (mm)	FTD (%)	Fill gas (bars)	LHGR (kW/m)	Enr. Wt/%	EOL burnup ($MWd/kgUO_2$)
{ }	0.07	10.850	1.80	95.00	1.0	25	10.0	32.19
{ }	0.20	10.590	1.80	95.00	1.5	20	9.93	35.76
{ }	0.10	10.700	1.80	95.00	1.0	30	10.0	34.09
{ }	0.05	5.560	1.80	96.76	10.0	16	11.5	19.30
{ }	0.18	8.040	1.80	95.50	10.0	10	3.5	21.28
{ }	0.13	8.090	1.80	95.50	10.0	10	3.50	23.66
{ }	0.07	10.590	2.04	94.00	1.0	25	3.95	11.37
{ }	0.10	5.915	2.00	94.00	10.0	25	13.0	50.57

b) The fuel density correction (Eqs. 10.3.4 and 10.3.5) is an empirical model that provides SIMULATE5 with the main practical consequence of the high burnup rim, *i.e.,* an increase in the fuel thermal diffusivity due to the thermal barrier imposed by the added porosity.

The empirical correction is a two-step approach:

Step 1 relates the reduction in the pellet density (due to the added {rim porosity}) to the excess average pin burnup above {40} MWd/kgU,

$$\left\{ \qquad \right\} \qquad \text{Eq. 1}$$

Step 2: The reduction in the pellet density (r_p) is subtracted from the as-fabricated density (d) to evaluate the density correction in the Nuclear Fuel Industries correlations.

$$d^* = d - r_P \qquad \text{Eq. 2}$$

where d^* is the effective pellet density (fraction of TD). The added rim porosity reduces the fuel thermal conductivity.

The Halden rods were not used to derive the constant { } on Eq.1. There is not enough information in the Halden rods available to Studsvik Scandpower. There is only one rod with EOL burnup above { } MWd/kgU; furthermore, its geometry is not representative of a typical LWR fuel rod.

Instead, SIMULATE5's fuel pellet average temperature predictions were compared against the solution of a reference fuel performance code for a few typical LWR rods. The figure below shows one of such comparisons for a PWR 17×17 fuel rod. The average fuel temperature rise above the coolant temperature is shown as a function of burnup for a constant linear heat generation rate of { } kW/m. The blue line represents the SIMULATE5 solution *without* the rim effect correction (*i.e.* the UO_2 thermal conductivity was computed using the *as-fabricated* density *d*) and the red line represents the reference solution.

After { } MWd/kgU, the pellet-cladding gap closes and the fuel thermal conductivity governs the thermal resistance between the fuel rod and the coolant. Note that, (1) the SIMULATE5 solution predicts a { } of the average fuel temperature, and (2) the reference solution predicts an { } variation of the fuel temperature with burnup. The { } of the SIMULATE5 solution is a direct consequence of the burnup dependence of the Nuclear Fuel Industries correlations[1].

In order to increase the fuel temperature predicted by SIMULATE5 at high burnup, the fuel thermal conductivity must be reduced under such conditions. At the same time, it is not desirable to change the fuel thermal conductivity at low burnups. The effective density empirical correction does exactly that.

The next figure shows the effect of the empirical correction. The blue line represents the SIMULATE5 solution *with* the rim effect (*i.e.,* the UO_2 thermal conductivity was computed using the effective density d^*) and the red line represents the reference solution.

[1] The UO2 thermal conductivity functionality looks like $k_{UO2} \approx \frac{1}{a + b \cdot T + c \cdot Bu}$

Note that the differences between the SIMULATE5 solution and the reference solution have been reduced for burnups greater than { } MWd/kgU. For example, at { } MWd/kgU the difference was reduced from ~{ }K to ~{ }K.

The next figure compares the two SIMULATE5 solutions, *i.e.,* with the as-fabricated density (red line) and with the effective density (blue line).

Note that:

- Fuel temperature differences are less than { } K.
- The effective density correction is only significant if the rod average burnup is { } MWd/kgU or higher.
- The differences observed in the previous figure are over-estimated at high burnup because the calculations were performed at a *constant linear heat generation rate*. In reality, the power generated in a rod will be reduced at high burnup.

References:

1. Kolstad, E. and F. Sontheimer, "Fuel Thermal Conductivity Changes with Burnup as Derived from In-Pile Temperature Measurements," HWR-299, Halden, Norway (1991).
2. Alvarez, M.T., M. Haral, and W. Wiesenack, "Analysis of the Thermal Behavior of Gd-Bearing Fuel in IFA-515," HWR-470, Halden, Norway (1996).

7. For the gaseous conductance model in SIMULATE5 (Section 10.3.3 Equation 10.3.10) the gas conductivity is expressed as a function of [fuel burnup, an effective fuel pellet radius, and the thermal conductivities of xenon, krypton, and helium gases] Explain the basis and formulation of the[proportionality constant { } and the effective fuel pellet radius (r_{fp})].

The empirical correction (Eq. 10.3.10) reduces the conductivity by the presence of fission products (Kr, Xe) in the gas. Two assumptions were made:

- The correction is independent of plenum or gap volume.
- The correction is assumed proportional to fuel volume and burnup.

The proportionality constant { } was determined using an INTERPIN calculation for an LWR lattice with a fuel pin radius of { } cm. The calculations were performed to a burnup of { } MWd/kg at a constant liner heat generation rate of { } kW/m. From the INTERPIN calculation, one can extract the gap size and the gap conductance as a function of burnup.

{

}

The product of the gap size and the gap conductance can be used to estimate the gas thermal conductivity as a function of burnup. The gas thermal conductivity degradation is estimated by dividing the gas thermal conductivity at burnup *Bu* by the initial value of the gas thermal conductivity.

It is important to note that after a burnup of { } MWd/kgU, there are other mechanisms that significantly impact the heat transfer between the pellet and the cladding. Therefore, the INTERPIN solution in the range { } MWd/kgU will be used to estimate the gas thermal conductivity degradation. The next figure shows the estimated thermal conductivity degradation (blue line) and the result of Eq. 10.3.10 (orange line).

{

}

It is important to mention that the SIMULATE5 average fuel temperature solution is {rather insensitive} to the actual value of the proportionality constant. This is demonstrated by the following sensitivity study for a PWR 15×15 rod with a linear heat generation rate of { } kW/m.

The study considers three cases:

- *Base case*: the default gas conductivity degradation curve will be used (constant set to { })
- *Gas thermal conductivity degradation is ignored:* the proportionality constant is set to { }
- *Gas thermal conductivity degradation is enhanced*: the proportionality constant is set to { }

The figure below shows the behavior of the gas thermal conductivity degradation factor (Eq. 10.3.10) for the cases under consideration,

Base case

The figure below compares the SIMULATE5 solution with the default constant { } against a reference solution obtained with a fuel performance code. The blue line represents the SIMULATE5 solution and the red line represents the reference solution.

Gas thermal conductivity degradation is ignored

The figure below compares the SIMULATE5 solution without gas thermal conductivity degradation (constant = { }) against a reference solution obtained with a fuel performance code. The blue line represents the SIMULATE5 solution and the red line represents the reference solution.

Gas thermal conductivity degradation is enhanced

The figure below compares the SIMULATE5 solution with enhanced gas thermal conductivity degradation (constant = { }) against a reference solution obtained with a fuel performance code. The blue line represents the SIMULATE5 solution and the red line represents the reference solution.

Comparison of SIMULATE5 solutions

The figure below compares the SIMULATE5 base case (constant = { }) with the case for which the degradation is ignored (see left side of the figure) and with the case for which the degradation is enhanced (right side). The red line represents the SIMULATE5 base solution and the blue lines represent the solutions with different degradation constants.

Gas Thermal Conductivity Degradation Ignored/Reduced (constant = { })	**Gas Thermal Conductivity Degradation Enhanced (constant = { })**
Differences TFU Gap Average(0:60) { } { } Minimum(0:60) { } { } Maximum(0:60) { } { }	Differences TFU Gap Average(0:5:60) { } { } Minimum(0:5:60) { } { } Maximum(0:5:60) { } { }

Note that the maximum differences between the base solution and the two extreme cases are less than { }K for the predicted fuel average temperature. The differences in the fuel average temperature are due to differences in the temperature rise across the fuel / cladding gap.

8. The following questions are related to the methodology and calculations performed for nuclear uncertainty factor (NUF) determination.

Provide *details* on the NUF factor generation methodology:

- **Details on the statistical analysis for tolerance limit determination**
- **Details on the 95/95 one-sided tolerance limit determination**
- **Details on the non-parametric tolerance limit calculations**

In order to provide specific details on the determination of tolerance limits and NUFs, a worked example recreating tolerance limits/NUFs from SSP-14/P01-028-TR is presented. The step-by-step process to determine the "Combined" Core Reactivity Tolerance Limits and NUFs summarized in Table 4-17 is given using the equations cited in Section 3.3 of the topical report. Any equation numbers cited refer to the equation numbers given in the SSP-14/P01-028-TR topical report.

Step 1 – Compute Difference Data

The first step is to determine the difference between the predicted value and the measured value for each of the 3256 observations available from the benchmark comparisons (i.e. for the combined data set from Plants A through E). For determining the Core Reactivity tolerance limits, the absolute difference (as opposed to relative or percent difference) between predicted and measured critical boron concentrations is calculated using eq. 3.1. Note that as stated in the topical report, the differences in boron concentration (ppm) units have been transformed into differences in reactivity (pcm) using predicted boron worth coefficients.

The following table presents examples of the difference calculation for selected observation points within the 3256 Core Reactivity data set:

Observation Number	Predicted Boron Concentration (ppm)	Measured Boron Concentration (ppm)	Absolute Difference calculated using eq. 3.1 (ppm)	Predicted Boron Worth* (pcm/ppm)	Absolute Difference (pcm)
1	.	.	.	.	.
2	.	.	.	.	.
3	.	.	.	.	.
.	1365	1372	-7.0	6.24	-44
.	1333	1343	-9.8	6.31	-62
.	1333	1343	-10.2	6.31	-64
3254	.	.	.	.	.
3255	.	.	.	.	.
3256	.	.	.	.	.

*Note – Boron worths are normally negative values, but these boron worths are given as magnitudes only to preserve the sense of the (predicted – measured) differences.

Step 2 – Compute Summary Statistics

The average (arithmetic mean) and sample standard deviation for this data set are calculated using equations 3.3 and 3.4 of the topical report. In this worked example "N" is equal to 3256 observations. For both calculations the values being operated on come from the last column of the table in Step 1 above.

Average = $\bar{X}$ = 23 pcm

Sample Standard Deviation = s= 93 pcm

These values are the same ones reported in Table 4-9 of the topical report on the "Combined" row.

Step 3 – Test for Normality

To test whether or not the data set is normally distributed, the method described in SSP-14/P01-028-TR Section 3.3.6 is used. In practice, any software that has the AS R94 implementation of the Shapiro-Wilk test can be used to test a data set for normality. In the example below, sample commands are given for the free, public domain software Dataplot developed by the National Institute of Standards and Technology (NIST).

In this worked example, all 3256 Core Reactivity Absolute Difference values have been placed in a file (one value per row) called "All_CBC_NUF.obs".

The following Dataplot commands are issued after starting Dataplot:

```
> READ All_CBC_NUF.obs Y
> WILKS SHAPIRO NORMALITY TEST Y
```

which produces the output on the following page.

As stated in the topical report, the significance level of 0.01 is selected for this test, which corresponds to a confidence level of 0.99 or 99%. Based on the Dataplot Conclusions section of the output on the next page, it is seen that the null hypothesis of "Normal" is rejected at the 99% confidence level (see highlighted row).

At this point the analyst would normally proceed directly to constructing tolerance limits using non-parametric methods, since the assumption of normality was rejected. In order to fully demonstrate all tolerance limit determination details however, the next step will construct tolerance limits assuming the null hypothesis of normality was accepted.

Example of Dataplot Output of the Shapiro-Wilk Normality Test

Wilk-Shapiro Test for Normality

Response Variable: Y

H0: The Data Are Normally Distributed
Ha: The Data Are Not Normally Distributed

Summary Statistics:
Total Number of Observations: 3256
Sample Mean: 22.84041
Sample Standard Deviation: 92.86482
Sample Minimum: -261.4500
Sample Maximum: 331.0000

Test Statistic Value: 0.9686091
P-Value: 0.4195664E-25

Conclusions

Null Hypothesis	Null Hypothesis Confidence Level	Acceptance Interval	Null Hypothesis Conclusion
Normal	50.0%	(0.500,1)	REJECT
Normal	80.0%	(0.200,1)	REJECT
Normal	90.0%	(0.100,1)	REJECT
Normal	95.0%	(0.050,1)	REJECT
Normal	97.5%	(0.025,1)	REJECT
Normal	99.0%	(0.010,1)	REJECT
Normal	99.9%	(0.001,1)	REJECT

Step 4 – "What if" scenario, Construct Tolerance Limits Assuming Normality

As discussed in Step 3, the assumption of normality was rejected, so non-parametric methods will be used to construct the tolerance limits. In order to fully describe all tolerance limit derivation methods used in SSP-14/P01-028-TR, it is instructive to assume for a moment that the null hypothesis of normality had been upheld for this exercise.

As described in Section 3.3.7 of SSP-14/P01-028-TR, the following equations (3.5 and 3.6) are used for determining tolerance limits for normal distributions:

$$Lower\ Tolerance\ Limit = TL_L = \overline{X} - (K * s)$$

$$Upper\ Tolerance\ Limit = TL_U = \overline{X} + (K * s)$$

Values for $\bar{X}$ and s (23 pcm and 93 pcm, respectively) were determined in Step 2. K, the 95/95 one-sided tolerance multiplier is determined using equations 3.7 and 3.8 from the topical report:

$$K = \frac{t(\gamma, N-1, \delta)}{\sqrt{N}}$$

$$\delta = z(0.95)\sqrt{N} = 1.645 * \sqrt{3256} = 93.87$$

$$K = \frac{t(0.95, 3255,\ 93.87)}{\sqrt{3256}}$$

To determine the numerator of the above equation, which is the inverse cumulative distribution function for the non-central t distribution, a Dataplot function is used:

>LET t = NCTPPF(0.95,3255, 93.87)

which returns:

THE COMPUTED VALUE OF THE CONSTANT T = 0.9643822E+02

Therefore:

$$K = \frac{96.438}{\sqrt{3256}} = 1.69$$

And the tolerance limits are computed as:

$$Lower\ Tolerance\ Limit = TL_L = 23 - (1.69 * 93) = -134\ pcm$$

$$Upper\ Tolerance\ Limit = TL_U = 23 + (1.69 * 93) = +180\ pcm$$

To continue this "what if" scenario a little further, the construction and application of Nuclear Uncertainty Factors (NUFs) from the tolerance limits derived by assuming normality is as follows:

A lower tolerance limit of -134 pcm implies that the CMS system underpredicts reactivity by no more than 134 pcm on a 95/95 statistical basis (recall differences are calculated as predicted – measured). That means if analyzing a design parameter where it is limiting to have too much reactivity, at least 134 pcm of reactivity must be added to any prediction of reactivity given by CMS. Therefore +134 pcm becomes the Upper NUF for this parameter.

Conversely, the upper tolerance limit implies that the CMS system overpredicts reactivity by no more than 180 pcm on a 95/95 statistical basis. So if analyzing a design parameter where it is limiting to have too little reactivity, at least 180 pcm must be subtracted from any prediction of reactivity given by CMS. Therefore -180 pcm becomes the Lower NUF for this parameter.

Step 5 – Construct Tolerance Limits Using Non-Parametric Method

Returning to the actual example from the topical report, the assumption of normality was not confirmed for the dataset of core reactivity differences, so tolerance limits must be constructed using the non-parametric method described in section 3.3.8.

The first task is to sort the 3,256 values of difference data from most negative to most positive.

Then equation 3.10 is used to find the mth value bounding 95% of the population with a 95% confidence level. Equation 3.10 for this specific problem is:

$$0.95 \leq I_{0.05}(m, 3256 - m + 1)$$

and is solved iteratively by increasing the integer value of "m" until the equation is no longer satisfied. The desired mth value would be the highest value that still satisfies the equation. The Excel BETADIST function can be used to evaluate equation 3.10:

$$0.95 \leq \text{BETADIST}(0.05, m, (3256 - m + 1))$$

Evaluated for several values of "m"…

$$\text{BETADIST}(0.05, 142, (3256 - 142 + 1)) = 0.959$$
$$\text{BETADIST}(0.05, 143, (3256 - 143 + 1)) = 0.951$$
$$\text{BETADIST}(0.05, 144, (3256 - 144 + 1)) = 0.942$$

…from these results, an "m" value of 144 is too large because 0.942 is not greater than or equal to 0.95. The "m" value of 143 is the largest integer value that still satisfies the equation. The lower tolerance value is now simply selected as the 143rd most negative sorted value, and the upper tolerance limit is the 143rd most positive sorted value. From the partial table presented on the next page, these correspond to:

$$Lower\ Tolerance\ Limit = TL_L = \{\quad\} \text{ pcm}$$
$$Upper\ Tolerance\ Limit = TL_U = \{\quad\} \text{ pcm}$$

Sorted List of Difference Data, Along with Most Negative and Positive Rankings

Most Negative Rank	Most Positive Rank	Sorted Difference Data List (pcm)
1	3256	-261
2	3255	-207
3	3254	-205
.	.	.
.	.	.
.	.	.
142	3115	{ }
143	3114	{ }
144	3313	{ }
.	.	.
.	.	.
.	.	.
3113	144	{ }
3114	143	{ }
3115	142	{ }
.	.	.
.	.	.
.	.	.
3254	3	289
3255	2	293
3256	1	331

Step 6 – Transform Tolerance Limits Into Nuclear Uncertainty Factors

A lower tolerance limit of { } pcm implies that the CMS system underpredicts reactivity by no more than { } pcm on a 95/95 statistical basis (recall differences are calculated as predicted – measured). That means if analyzing a design parameter where it is limiting to have too much reactivity, at least { } pcm of reactivity must be added to any prediction of reactivity given by CMS. Therefore { } pcm becomes the Upper NUF for this parameter.

Conversely, the upper tolerance limit implies that the CMS system overpredicts reactivity by no more than { } pcm on a 95/95 statistical basis. So if analyzing a design parameter where it is limiting to have too little reactivity, at least { } pcm must be subtracted from any prediction of reactivity given by CMS. Therefore { } pcm becomes the Lower NUF for this parameter.

Conclusion

By recreating the calculation of tolerance limits and NUF values for Core Reactivity from Table 4-17 of the topical report, extensive details for constructing 95/95 one-sided tolerance limits have been provided for normally distributed data sets and for data sets where no distribution is assumed (i.e. non-parametric), including details of the statistical treatment of the data for each case.

9. No details have been included in the submitted documents related to the topical report regarding the determination of nuclear reliability factors (NRFs) associated with neutronics/physics parameters. Please provide the basis, and their relationship of NRFs to the NUFs associated with the physics/neutronic parameters.

The Nuclear Reliability Factor (NRF) for a given physics parameter (e.g. core reactivity, control rod worth, etc.) is the allowance applied to CMS predictions for safety analysis calculations to ensure sufficient conservatism. The NRF is a value greater than or equal to the NUF determined for that parameter and is otherwise arbitrary. Although the NRF can be set exactly equal to the NUF, there are several reasons why it is desirable to make the NRF a larger value:

- The use of a NRF larger than its corresponding NUF allows for discretionary margin.
- Using a larger NRF value can allow for more convenient and memorable numbers. In the example presented in the response to question 8, the Core Reactivity lower NUF is { } pcm, and the upper NUF is { } pcm. By setting the NRF for this parameter to { } pcm (as was done in the topical report), a single convenient value is used for both upper and lower NRFs, which makes it easier to apply in safety analysis calculations.
- The topical report recognizes that software is changeable and provides a mechanism for managing the change (Section 3.7). This may mean that for a large change to the software the calculated NUFs also change for a given parameter. If the NRF is exactly equal to the NUF, even small changes to the NUF would necessitate updating all of the procedures, licensing documents (including potentially the Safety Analysis Report), and other documents or software that list the value of the uncertainty to apply to safety analysis calculations. If the NRF is instead selected to be somewhat larger than the originally calculated NUF, any change to the NUF due to a change to the software simply needs to be evaluated to ensure it is still less than the NRF, resulting in fewer document and process updates.

10. Section 3.4.2 of SSP-14/P01-028 TR-P indicates that one of the ways to minimize the uncertainty in critical boron concentration is to restrict/assume a default value for B^{10}/B atom ratio of { } atom present. Explain the basis of this default value. Is this value realistic in actual reactor situations under normal, HZP, HFP and other operational transients?

Section 3.4.2 Item 2 is not intended to imply that uncertainty in critical boron concentrations comparisons is minimized by setting the default CMS5 ratio to any particular value. The statement about the default B10/B atom ratio of CMS5 being { } is simply a statement of the value assumed for cross section generation.

This sentence has been removed to improve the clarity of the final approved version. This Item now reads:

" 2. The B10 / B atom ratio of any particular boron sample can introduce uncertainty to the comparison if it is not accounted for. Strategies to reduce this uncertainty include: "

11. In the axial portion of the SIMULATE-5 solution technique (the first step), "the 1-D multi-group diffusion equation is solved in the subnode geometry for each assembly." Does this mean it is solved once to represent each subnode of a specific type (with the same axial materials), or is this step performed for literally every subnode in the calculation?

The 1-D multi-group diffusion equation in the subnode geometry is literally solved for each fuel assembly (1 node/assembly radial nodalization) or quarter of a fuel assembly (4 nodes/assembly radial nodalization) during each power/void iteration step.

The 1-D model divides the fuel assembly axially into "subnodes" such that cross sections are constant within each subnode. The boundaries of the subnodes coincide with the boundaries of the axially uniform original nodes, the spacers, the control rod zones, and the fuel material zones. Boundary conditions are provided by the bottom and top albedos. The influence of neighboring assemblies is handled by converting the radial leakage, known from the most recent Power/Void iteration of the global 3D solution.

12. In SIMULATE5, the 2D diffusion equation is solved one axial plane at a time. Does this imply that the axial spatial discretization has to be consistent across the core?

Yes, the axial spatial mesh used as the axial planes of the 2D diffusion solver as well as with the 3D global solver are consistent and uniform across the core. The user defines the number of uniform axial fuel nodes in the model. Note that SIMULATE5 internally uses a more detailed axially non-uniform mesh, which may also vary from one assembly to the other in the core. The internally-defined axial mesh is used with the 1-D axial homogenization model and the depletion model, which tracks the burnup/history and isotopic number densities. The flux shape obtained from the 1-D model is used for computing the axially homogenized cross-sections and axial discontinuity factors of the 3D global solver and the axially homogenized cross sections of the 2D diffusion model.

13. In SIMULATE5, what assumptions are involved with representing the submesh equations in the finite difference-like format that is used to increase calculational efficiency of the submesh solution?

The submesh model solves the diffusion equation for a rectangular node size $h_x \times h_y$ as shown in the figure below:

$$-D\frac{\partial^2\phi}{\partial x'^2} - D\frac{\partial^2\phi}{\partial y'^2} + \Sigma_r\phi = Q(x', y') \qquad \text{Eq. 1}$$

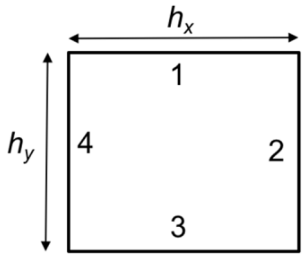

The source term on the right hand side includes both the fission and scattering source.

The simplest approximate solution to Eq. 1 would be based on the finite difference method which approximates the node side flux gradient by the node side flux and node average flux as:

$$\frac{d\phi}{d\xi} = \phi_{side} - \bar{\phi} \qquad \text{Eq. 2}$$

Eq. 2 has a nice property of giving rise to a final equation for the node average flux which is simple and robust and for which well-known iteration techniques can be applied. However, {the accuracy is poor}.

SIMULATE5's submesh model uses a more accurate expression for the side flux gradient which has a format reminiscent of Eq. 2.

First, the model assumes that the source term is a quadratic polynomial in x and y. Converting Eq. 1 to dimensionless coordinates:

{ } Eq. 3

where { }are the { } polynomials and

{ } Eq. 4

An approximate solution to Eq.3 is assumed as

Eq. 5

Eq. 6

The four unknown expansion coefficients K_i of Eq. 5 are found from four node boundary conditions (node average side fluxes). The c_i coefficients are evaluated by substituting Eq. 5 into Eq. 3 and matching terms.

After considerable algebra, the side average flux gradients are related to the side average flux, node average flux, and source expansion coefficients as

Eq. 7

and analogously for the y direction. It has been defined

Eq. 8

Eq. 9

Introduction of the auxiliary variables ψ, ε, μ_x and μ_y:

Eq. 10

Eq. 11

Eq. 12

Equation 7 can be written

Eq. 13

Eq. 13 is the sought for finite-difference like expression (c.f. Eq.2) for the side flux gradient. It is the basis for the EW (exponential waves) option of the SIMULATE5's submesh model. The ψ variable can be viewed as a fictitious midpoint (or driving) flux. If one views the x and y directions separately, (ψ-ε) can be viewed as driving flux in the y direction and ψ+ε in the x direction. Hence, the ε term is an in-streaming imbalance correction.

A simplified version of the nodal equation derived is obtained by making the following additional assumptions:

As a result, Eq. 13 transforms into

Eq. 14

for all sides. This relation must be complemented by an equation relating the fictitious midpoint flux, ψ, to the assembly average flux. As a first-order approximation, it can be shown that when flux expansion Eq. 5 is assumed, the node average flux is related to the side average flux in accordance with the following equation:

Eq. 15

where

Eq. 16

Eq. 14 is the basis for the PSI option of the submesh model.

14. For SIMULATE5, when correcting the initial nuclide number densities (N^{actual}) to correct for as-built enrichment and fuel weight, the term N_i^{SA} is used. What phenomena does this term represent, and how is it obtained?

SIMULATE5 methodology manual section 5.3 discusses the initialization of the actual isotopic number densities of the hybrid macro/micro cross-section model for the difference in design vs. manufacturing (as-built) in fuel assembly heavy metal loading and enrichment. The term N_i^{SA} used in Equations of 5.3.18 through 5.3.21 is the CASMO5 calculated initial isotopic number densities for fuel at zero burnup.

The single assembly number densities are then corrected for "as-built" heavy metal loadings.

(5.3.18)

Fuel heavy metal loadings are typically measured by assembly and not by segment. The second correction term, for segment loadings, is typically 1.0.

Optionally, the U234, U235, and U238 number densities are corrected for "as-built' enrichment for a fresh fuel assembly as shown below:

(5.3.19)

(5.3.20)

(5.3.21)

where:

N_i^{SA} Initial CASMO5 number density for nuclide-i

k Axial node index (the summation is over the entire height of the assembly)

v_k Volume of node k

{ } User input total { heavy metal loading }for an assembly

{ } CASMO5 {heavy metal loading} for segment in node-k

{ } SIMULATE5 as-built { } for segment in node-k ({ }unless segment { } is not overwritten via SEG.LOA card in SIMULATE5 input)

{ } CASMO5{ }

{ } SIMULATE5 { } (input through SEG.DAT card).

The as-built loading (common) and as-built enrichment (less common) options in SIMULATE5 allows the neutronic model to take into account the small variations (typically less than { }) in design vs manufacturing of the fuel without requiring a user to re-run an explicit CASMO5 segment calculation for each individual fuel assembly in the core. SIMULATE5 offers input options for as-built assembly and segment weights and segment U235 enrichment. It is not possible to compute the complete isotopic content of the fuel based on only available information (the weight and U-235 enrichment). Accordingly, the corrected number densities are { } CASMO5 number densities { } CASMO5 to SIMULATE5 loading and U-235 enrichment is shown in Eqs. 5.3.18-21.

15. In SIMULATE5 three options can be used for tracking Iodine and Xenon concentrations. Are the same options used for tracking Promethium and Samarium?

In SIMULATE5, promethium and samarium are tracked as part of the extended Sm chain. The chain contains {15} isotopes starting from Nd-147 and extending to Gd-155. The Sm depletion chain is solved with the conventional predictor/corrector method. In addition to using Pm/Sm isotopic number density as computed by the microscopic depletion model, the user can set the number density of Sm-149 to its peak or to zero.

In summary, S5 offers the following three Samarium calculation options:

1. Update Sm-149 by depletion
2. Peak Sm-149
3. Zero Sm-149

These options are the same as those for xenon and iodine concentrations except for option 2. For xenon and iodine, the second option is equilibrium.

16. In SIMULATE5 the transverse leakage is approximated with a parabolic shape, but it is also stated that the actual shape is known from the submesh calculations. Is the parabolic assumption used initially, and eventually replaced by the submesh shape? Are the two combined in some way?

It is correct that the detailed shape of the radial leakage is readily available from the solution of 2D diffusion equation in submesh geometry. However, this information is not directly used to describe the transverse leakage in the 3D global solver. The 2D submesh model is used primarily to compute radially homogenized cross-sections and discontinuity factors. When the discontinuity factors are computed from the 2D submesh model, it is important that the shape of the transverse leakage is constructed in the same manner in the radial submesh model as in the global 3D solver, equations which are derived with the assumption of the quadratic transverse leakage. Otherwise, the global solver would operate with a discontinuity factor that would not (in a clean 2D case) be able to reproduce the submesh results. Hence, the known detailed submesh results are not directly used (as would be possible) to construct a transverse leakage shape that is considerably more exact than the three-node parabola fit.

17. Why does SIMULATE5 perform the radial submesh calculation to get a flux shape when this shape should be already known from the CASMO5 submesh? Is the CASMO5 shape used as a starting point for the iteration process?

The submesh flux distribution from CASMO5 is only available for a single assembly with zero-net current boundary conditions. Although, the submesh fluxes of SIMULATE5 would ideally be the same as those of CASMO5 for a single node solution, they would be substantially different for the full 2D core geometry. Therefore, the CASMO5 submesh fluxes are only used as an initial guess when solving the single node and full 2D core solution of the submesh equations: CASMO5 fluxes are used as an initial guess for a single node problem, and they are scaled with nodal powers when initializing the full 2D core problem.

18. What histories and branching variables are typically varied in CASMO5 and subsequently used by SIMULATE5? Does radial submesh-wise data get processed by Core Management System (CMS) link and passed between the codes based on these histories and branches?

The standard CASMO5 case matrix (S5C input card) for a PWR fuel segment typically contains the following history and branch information:

Histories are run for:

- Boron (HBOR),
- Moderator Temperature, (stored as moderator density) (HTMO),
- Fuel Temperature (HTFU),
- Control Rods (HCRD).

Branch cases are run for:

- Shutdown Cooling (SDC),
- each type of Spacer Grid,
- Xenon,
- Combinations of Boron (BOR) and Moderator Temperature (TMO), Control Rods (CRD) and Moderator Temperature (TMO), Fuel Temperature (TFU) and Moderator Temperature (TMO).

The CASMO5 user's manual pages for the S5C card in Section 2.1 describe this in more detail.

The { } data is also processed by CMSLINK5 along with the { }. Its functionalization is essentially the { }. The { ,} is to use a { }.

19. The three-step solution process 3D solver, axial and radial homogenizations is iterative by nature, feeding a number of parameters into each other until convergence. During the first iteration, how are parameters that have not yet been determined initialized? Does this have any effect on the final solution?

Both the axial and radial homogenizations are performed inside the power/void (moderator density) loop. The initialization of each model is as follows:

1-D Axial Homogenization: The axial homogenization is carried out once the subnode cross sections are known. During the first power/void iteration, the subnode fluxes are estimated solving the 1D multi-group diffusion equation based on the Finite Difference approximation. Other than the first power/void iteration, the subnode fluxes from the previous power/density iteration are used. During the first iteration, { }

2-D Radial Homogenization: During the first power/void iteration, the radial re-homogenization is skipped. It is performed during the second power/void iteration, which has better converged flux weight functions from the 1-D channel solver and axial-leakage from the 3D Global solution. During the first radial homogenization sweep, the single node problem submesh fluxes are initialized with CASMO5 submesh fluxes, and the 2D full core problem submesh fluxes are initialized with nodal power scaled CASMO5 submesh fluxes. Other than the first iteration sweep, { }.

Once the assembly homogenized cross-sections are corrected for the axial and radial heterogeneities, the 3-D diffusion equation is solved to obtain node average fluxes and surface fluxes/currents. The 3-D solver provides feedback to the 1-D and 2-D solvers via the radial and axial leakage terms. The non-linearity introduced by axial and radial homogenization models are { } compared to the thermal-hydraulic non-linearity, and convergence difficulties have not been observed. Since all three steps are repeated during each power/void iteration until the requested eigenvalue and flux convergence attained with the 3D global solver, the final solution is insensitive to the initialization of the parameters of the models.

20. For the tank critical assembly reflector experiment CASMO5 Eigenvalue results listed in Table 3-11 (SSP-14-P01/012) the eigenvalue and the delta increases with increase in steel reflector thickness as well as for increase in steel/water thickness. Explain the implications of this increase when the CMS code system is used for the modeling and analysis of PWR cores.

The TCA critical facility configuration involves a single 15x15 PWR fuel assembly with significant fast neutron leakage. Therefore, an otherwise small bias in eigenvalue in a full-core model due to the presence of a heavy steel reflector is greatly magnified by the TCA experiment. Furthermore, the maximum difference between the predicted critical and measured critical height is approximately { } pcm – well within the expected range of some critical experiment differences. Extensive experience and comparisons to core-follow CMS5 models indicates that the current approach is valid for PWR reflectors involving baffle and barrel structural regions.

21. In Tables 4-2 through 4-8, the end of cycle burnup is labelled GWD/MTU, but the values are listed in MWD/MTU. Please correct either the values or the label for burnup.

The labels have been corrected for each table. Below each corrected table is provided as it will be inserted into the approved version of SSP-14/P01-028-TR-P-A.

Table 0-3: Plant "A" (Westinghouse 2-Loop)
Benchmark Cycle Details
(7 Cycles)

Cycle	Thermal Rating (MWt)	Absorber Type	Reload Pellet Enrichment Range	End of Cycle Burnup (GWD/MTU)
A1C26	1650/1772	Gadolinia	2.60-4.95	17.400
A1C27	1772	Gadolinia	2.60-4.92	16.977
A1C28	1772	Gadolinia	2.60-4.95	17.856
A1C29	1772	IFBA	2.60-4.40	18.460
A1C30	1772	IFBA	2.60-4.90	18.124
A1C31	1772	IFBA	2.60-3.70	13.837
A1C32	1772	IFBA	2.60-4.90	13.325

**Table 0-4: Plant "B" (Combustion Engineering 2-Loop)
Benchmark Cycle Details
(10 Cycles)**

Cycle	Thermal Rating (MWt)	Absorber Type	Reload Pellet Enrichment Range	End of Cycle Burnup (GWD/MTU)
B2C14	2700	Gadolinia	0.72-4.30	19.062
B2C15	2700	Gadolinia	2.15-4.43	16.105
B2C16	2700	Gadolinia	2.20-4.40	15.182
B2C17	2700	Gadolinia	2.15-4.30	15.383
B2C18	2700	Gadolinia	2.25-4.50	15.649
B2C19	2700	Gadolinia	2.25-4.50	14.796
B2C20	2700	Gadolinia	2.20-4.30	15.182
B2C21	2700	Gadolinia	2.20-4.25	15.201
B2C22	2700	Gadolinia	2.20-4.35	15.336
B2C23	2700	Gadolinia	2.20-4.35	15.428

**Table 0-5: Plant "C" (Westinghouse 4-Loop)
Benchmark Cycle Details
(6 Cycles)**

Cycle	Thermal Rating (MWt)	Absorber Type	Reload Pellet Enrichment Range	End of Cycle Burnup (GWD/MTU)
C3C11	3411	IFBA	2.60-4.95	20.017
C3C12	3411	IFBA	2.60-4.95	19.770
C3C13	3650	IFBA	2.60-4.90	20.041
C3C14	3650	IFBA	2.60-4.95	20.845
C3C15	3650	IFBA	2.60-4.95	20.970
C3C16	3650	IFBA	2.60-4.95	20.536

**Table 0-6: Plant "D" Unit 1 (Westinghouse 3-Loop)
Benchmark Cycle Details
(10 Cycles)**

Cycle	Thermal Rating (MWt)	Absorber Type	Reload Pellet Enrichment Range	End of Cycle Burnup (GWD/MTU)
D1C15	2893	B4C	4.15-4.25	20.021
D1C16	2893	B4C	4.25-4.40	19.829
D1C17	2893	B4C	4.45-4.55	19.815
D1C18	2893	B4C	4.25-4.55	20.503
D1C19	2893	B4C	4.50-4.55	20.416
D1C20	2893	B4C	4.45-4.55	20.057
D1C21	2893/2940	B4C	4.40-4.55	20.343
D1C22	2940	B4C	4.55	16.420
D1C23	2940	IFBA/WABA	3.65-4.40	19.812
D1C24	2940	IFBA	4.55	20.027

**Table 0-7: Plant "D" Unit 2 (Westinghouse 3-Loop)
Benchmark Cycle Details
(10 Cycles)**

Cycle	Thermal Rating (MWt)	Absorber Type	Reload Pellet Enrichment Range	End of Cycle Burnup (GWD/MTU)
D2C14	2893	B4C	4.15-4.25	19.809
D2C15	2893	B4C	4.15-4.25	18.333
D2C16	2893	B4C	4.30-4.45	17.866
D2C17	2893	B4C	4.25-4.40	19.156
D2C18	2893	B4C	4.20-4.40	19.705
D2C19	2893	B4C	4.50-4.55	19.012
D2C20	2893	B4C	4.25-4.50	19.249
D2C21	2940	B4C	4.25-4.45	17.891
D2C22	2940	B4C	4.25-4.45	19.454
D2C23	2940	IFBA/WABA	3.80-4.45	18.757

**Table 0-8: Plant "E" Unit 1 (Westinghouse 3-Loop)
Benchmark Cycle Details
(10 Cycles)**

Cycle	Thermal Rating (MWt)	Absorber Type	Reload Pellet Enrichment Range	End of Cycle Burnup (GWD/MTU)
E1C16	2546	B4C	4.10-4.25	17.544
E1C17	2546	B4C	4.10-4.25	18.072
E1C18	2546	B4C	4.10-4.25	16.783
E1C19	2546	B4C	4.10-4.25	17.004
E1C20	2546	B4C	3.80-4.10	17.092
E1C21	2546	B4C/IFBA	3.80-4.25	17.709
E1C22	2546	IFBA	3.60-4.25	17.398
E1C23	2546	IFBA	3.90-4.25	18.518
E1C24	2587	IFBA	3.65-4.10	18.348
E1C25	2587	IFBA	3.75-4.00	17.868

**Table 0-9: Plant "E" Unit 2 (Westinghouse 3-Loop)
Benchmark Cycle Details
(10 Cycles)**

Cycle	Thermal Rating (MWt)	Absorber Type	Reload Pellet Enrichment Range	End of Cycle Burnup (GWD/MTU)
E2C16	2546	B4C	3.80-4.25	16.649
E2C17	2546	B4C	4.10-4.25	16.877
E2C18	2546	B4C	4.10-4.25	17.735
E2C19	2546	B4C	4.10-4.25	17.482
E2C20	2546	B4C	4.10-4.25	17.540
E2C21	2546	B4C/IFBA	3.70-4.25	18.296
E2C22	2546	IFBA	3.65-4.25	18.532
E2C23	2546	IFBA	3.65-4.10	16.937
E2C24	2587	IFBA	3.95-4.05	17.702
E2C25	2587	IFBA	3.85-4.10	17.876

22. Provide details of the configuration, system description, fuel types, poison loadings, moderator types used, methodologies employed, and results and comparisons for the following benchmarks/experiments:

a. C5G7 benchmark
b. S5C Case Matrix
c. KRITZ3 Experiments
d. TCA Reflector
e. MCNP6 Comparisons

a. C5G7 2D Benchmark Calculation with CASMO5

An OECD benchmark described in Reference 1 has been performed in CASMO5 to demonstrate the accurate implementation of the transport solution within the code, Reference 2.

The benchmark uses the 2D C5 computation geometry, which is a 17x17 fuel assembly lattice to construct a 16 assembly ¼ core symmetric geometry (Figure 1). The cross-sections are supplied in the benchmark consisting of a 7 energy group structure.

The results of the benchmark calculation and comparisons to reference values are shown in Tables 1 through 3. The errors in Table 1 are calculated using Equation 1. The very good agreement demonstrates that the transport method has been implemented correctly in CASMO5.

$$Percent\ Relative\ Error = \frac{(CASMO5 - Reference)}{Reference} * 100 \qquad (1)$$

Figure 1: C5G7 Benchmark Geometry

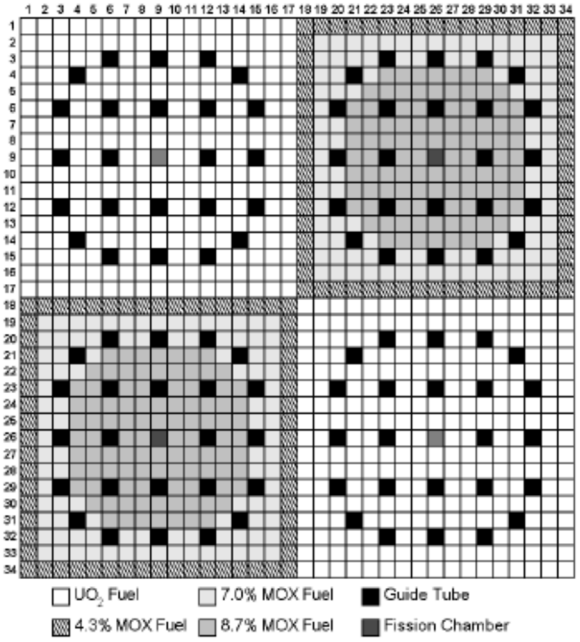

Table 1: CASMO5 C5G7 Eigenvalue Comparison

Code	$K_{effective}$
CASMO5	1.18650
MCNP4.1 (Ref)	1.18655

Table 2: CASMO5 C5G7 Power Distribution Comparison

% Error at the Maximum Pin Power Location	% Error at the Minimum Pin Power Location	Maximum % Error at any Location	% Error of Assembly Powers*
0.033	0.304	0.509	UO2 Inner = 0.034 MOX = -0.0013 UO2 Outer = -0.115

* Inner is defined as the NW assembly and outer is the SE from Reference 1.

Additional statistical quantities were defined in the benchmark to be calculated as a means to evaluate the quality of the power distribution calculation as a whole. These are shown in Table 3, with the definitions stated in Equations 2 and 3.

Table 3: CASMO5 C5G7 Power Distribution Statistics

Average Absolute Value Error	RMSE	MRE
0.134	0.005	0.110

$$RMSE = \sqrt{\frac{1}{N}\sum_{i=1}^{N}(CASMO5_i - Reference_i)^2} \quad (2)$$

$$MRE = \frac{\sum_N |e_n| * p_n}{N * p_{avg}} \quad (3)$$

References:

1. NEA/NSC/DOC(2003)16 "Benchmark on Deterministic Transport calculations without spatial homogenization A 2-D/3-D MOX fuel assembly Benchmark", ISBN 92-64-02139-6

2. B. Haugh, "C5G7 2D Benchmark Calculation with CASMO5," SSP-14-P01/006-C, 2014

b. S5C Case Matrix Validation

Reference 1 assesses the accuracy of the S5C case matrix that is implemented in CASMO5 for use in the Core Management Suite (CMS5) software.

The analysis examined the S5C case matrix for PWRs. The types of single assembly calculations that were performed are:

- Pin lattice geometries ranging from 14x14 to 17x17 including both large and small water hole designs.
- Integral burnable absorbers types: Gadolinia (Gd_2O_3) and IFBA (ZrB_2).
- Discrete absorber types: WABA, B_4C-AlO_3, Boron Silicate Glass and Hafnium Suppression Rods.
- Control Rod absorber types: B_4C, Ag-In-Cd, W and Hafnium.
- Low enriched Uranium Oxide (UO_2) fuel.
- Soluble Boron in the coolant.

The comparison between exact conditions calculated in CASMO5 and those calculated in SIMULATE5 using cross-sections from the S5C case matrix will be performed using the {audit} function in SIMULATE5.

The { } function will be used to assess how the case matrix performs from two different perspectives. The first perspective is how the case matrix performs for PWR operational and safety analysis conditions. The second is how well the interpolation (and some extrapolation) performs between and beyond the actual S5C calculated statepoints.

Typical PWR operational condition Audit Matrix:

The purpose of this audit matrix was to investigate the statepoint space where a typical PWR would operate. These conditions are largely derived from experience in determining the inputs to the safety analysis for different US PWR's.

The operational conditions can be divided into different sections.

1) Normal PWR operation, cold to hot full power.
2) PWR non-LOCA accidents, both rodded and unrodded.
   a. Rod Ejection
   b. Rod Withdrawal
   c. Locked Rotor
   d. Dropped Rod
   e. Large and Small Steam Line Breaks
3) Other PWR Events
   a. Shut Down Cooling Effects
   b. Cold Xenon Free Conditions for Refueling Boron and Startup Predictions

To accomplish this, a case matrix is chosen to use base conditions that represent a typical PWR and then to perturb those base conditions over the range of operational and non-LOCA accident scenarios. While the exact values that occur at different plants under different conditions will vary, they would be within the range of the analysis.

The representative base conditions chosen for these analyses are:

- Average Moderator Temperature (TMO) ={ }
- Average Fuel Temperature (TFU) = { }
- Average Soluble Boron Concentration (BOR) ={ }

From these base conditions, perturbations are performed. These use the COE cards and dependencies within CASMO5 inputs. The matrix is most easily split into nine regions that are discussed below.

Region 1

The region one cases are described using the following input cards:

```
BOR={          }  TMO={          }  TFU={          }   * At Power ARO perturbations
```

The input ranges were picked as representative of at-power operational conditions with some additional range. The TMO values range from { } to { } which encompass the inlet to outlet conditions of a typical at-power PWR. The average fuel temperature (TFU) values range from { }, which encompass very low power to at-power rod conditions in the reactor during normal operation. The BOR values range from { } ppm to { }ppm, representing the end of cycle with no boron to the beginning of cycle shutdown boron levels.

Somewhat non-physical conditions are examined where combinations of { } are calculated since the COE card performs the combination of all the variables listed at all depletion points in this case (default values of { } GWD/MTU are the maximum exposure points).

Region 2

Region two is described with the following input cards:

```
ROD='CRD'                                                    * At Power Rodded perturbations
BOR={              }  TMO={            }  TFU={            } ROD='CRD'
```

The input ranges are the same as region one but with the addition of instantaneous rod insertion using the ROD card. In this case the control rod used for control rod history is inserted from the choice of the ID of 'CRD'. For reactor types with multiple potential control rod absorber types a unique CASMO5 case is run for each one.

Region 3

Region three is described with the following input cards:

```
SDC={                              }/'H'                      * Shut down cooling cases
```

This region looks at the shutdown cooling accuracy. The choice of hours covers a wide range of outage lengths from short to very long. These are all from the base conditions.

Region 4

Region four is described with the following input cards:

```
TMO={    } TFU={    } BOR={                 }                 * Isothermal Conditions Unrodded
TMO={    } TFU={    } BOR={                 }
TMO={    } TFU={    } BOR={                   }
TMO={    } TFU={    } BOR={                  }
TMO={    } TFU={    } BOR={                  }
TMO={    } TFU={    } BOR={                   }
```

These perturbations are isothermal which sets the fuel and moderator temperatures to same value. The temperature range is from { } to { }, which represent cold shut down to hot zero power conditions over a range of boron conditions. These are also often initial conditions for various transients such as rod ejection and rod withdrawal events.

Region 5

Region five is described with the following input cards:

```
* Isothermal Conditions Rodded
TMO={    } TFU={    } BOR={               } ROD='CRD'
TMO={    } TFU={    } BOR={                } ROD='CRD'
TMO={    } TFU={    } BOR={                } ROD='CRD'
TMO={    } TFU={    } BOR={                } ROD='CRD'
TMO={    } TFU={    } BOR={                 } ROD='CRD'
TMO={    } TFU={    } BOR={                } ROD='CRD'
```

These are the same isothermal conditions as Region 4 but with instantaneous rod insertions of the control rod history rod type marked 'CRD'. These cold shut down to hot zero power conditions represent initial conditions for transients as mentioned above and also represent potential startup conditions at the higher range of temperatures.

Region 6

Region six is described with the following input cards:

```
* Zero Power Xenon Free Isothermal unrodded
XEN={ } PDE={ } TMO={    } TFU={    } BOR={               }
XEN={ } PDE={ } TMO={    } TFU={    } BOR={               }
XEN={ } PDE={ } TMO={    } TFU={    } BOR={                }
XEN={ } PDE={ } TMO={    } TFU={    } BOR={               }
XEN={ } PDE={ } TMO={    } TFU={    } BOR={               }
XEN={ } PDE={ } TMO={    } TFU={    } BOR={                }
```

These are the same perturbations as Region 4 but now with instantaneous xenon free and zero power states. These cases help examine how well the library will perform at initial conditions that are now xenon free for transients such as rod ejection and withdrawal.

Region 7

Region seven is described with the following input cards:

```
                                                * Zero Power Xenon Free Isothermal rodded
XEN={ } PDE={ } TMO={    } TFU={    } BOR={               } ROD='CRD'
XEN={ } PDE={ } TMO={    } TFU={    } BOR={               } ROD='CRD'
XEN={ } PDE={ } TMO={    } TFU={    } BOR={               } ROD='CRD'
XEN={ } PDE={ } TMO={    } TFU={    } BOR={               } ROD='CRD'
XEN={ } PDE={ } TMO={    } TFU={    } BOR={               } ROD='CRD'
XEN={ } PDE={ } TMO={    } TFU={    } BOR={               } ROD='CRD'
```

These are the same perturbations as in Region 5 but with instantaneous Xenon free and zero power states.

Region 8

Region eight is described with the following input cards:

```
                                              * Isothermal SDC Cases
TMO={    } TFU={    } BOR={     }            SDC={                          }/'H'
TMO={    } TFU={    } BOR={     }            SDC={                          }/'H'
                                              * Zero Power Xenon Free Isothermal SDC Cases
XEN={ } PDE={ }  TMO={    } TFU={    } BOR={     }  SDC={                       }/'H'
TMO={    } TFU={    } BOR={      }            SDC={                          }/'H'
```

These cases are isothermal shut down cooling branches at constant boron at near beginning-of-cycle concentration of { } ppm. They are initiated from conditions with and without Xenon.

Region 9

Region nine is the region that focuses on conditions that represent the initial or post transient conditions used to provide input to the safety analysis. While each vendor and utility may have slightly different methods and statepoints that are evaluated for these transients, these cases are representative. The inputs below are described for each event grouping.

Reactivity Initiated and Heat up events

These inputs describe the conditions that reactivity initiated and heat up events are evaluated at for a typical PWR. They are performed for both rodded and unrodded statepoints.

```
          TFU={             }  BOR={                 }             * Rod Ejection
TMO={    }  TFU={            }  BOR={                 }             * Rod Withdrawal
          TFU={             }  BOR={                 }             * Locked Rotor
          TFU={             }  BOR={                 }             * Dropped Rod Accident
```

Here the rod ejection event is modeled at base TMO conditions with varying TFU and boron.which represents potential PWR cores that could have limiting events at HZP or low power conditions that tend to be near base TMO. The fuel temperature and boron are varied to show reactivity effects from increasing TFU are appropriate. Boron variation is for time in cycle evaluation.

Rod withdrawal is modeled in a similar fashion with a slightly elevated TMO for the sake of examining some of the interpolation space and the increase in temperature for the low speed event. TFU is varied slightly on the high side as this slow event can result in higher average fuel temperatures.

Locked rotor events are evaluated with TMO now back at base conditions. TFU is slightly elevated above the rod ejection event as a result of how the heat up occurs during the transient and the time required to detect it with the reactor protection systems.

The dropped rod accident can be treated as a heat-up event if the steam control system has automatic control and compensates for the negative reactivity of the rod. The resulting power distribution in neighboring assemblies is now elevated, resulting in higher linear heat generation rates and higher TFU.

The input below shows the events repeated for rodded conditions; all other statepoint information is the same.

```
          TFU={             }  BOR= {                }  ROD='CRD'  * Rod Ejection (RODDED)
TMO={    }  TFU={              }  BOR={              }  ROD='CRD'  * Rod Withdrawal (RODDED)
          TFU={            }  BOR={                 }  ROD='CRD'  * Locked Rotor (RODDED)
          TFU={             }  BOR={                 }  ROD='CRD'  * Dropped Rod Accident
(RODDED)
```

Spectrum of Steam Line Breaks

The inputs below describe the conditions for a spectrum of steam line break events evaluated for a typical PWR. They are performed for both rodded and unrodded statepoints.

```
          TFU={             }  BOR= {                }             * Large Steam Line Break
          TFU={             }  BOR= {      }                     * Small Steam Line Break Check
TMO={    }  TFU={            }  BOR= {    }                     * Small Steam Line Break Check
TMO={    }  TFU={            }   BOR= {   }                     * Small Steam Line Break Check
TMO={    }  TFU={            }  BOR={             }            * Small Steam Line Break
```

The inputs above can be discussed in three groups. The first is the large steam line break that is evaluated at base TMO. The fuel temperature is varied from HZP/Tinlet conditions of { } to a high of { } representing the range from initial accident to maximum

power excursion. The boron conditions are varied from { } ppm, representing the range during the cycle and near shutdown conditions.

The second group is the small steam line break event. This event varies from the large break in how the transient would progress and could result in more limiting conditions. Here the statepoints are evaluated at a TMO representing near inlet temperature. The fuel temperature is varied in a similar manner to the large SLB with a higher maximum of { } representing a potentially more limiting event for the fuel. The boron concentrations are the same.

The last group are a series of small steam line breaks that are check for criticality from post-accident condition with lower TMO values and TFU values and zero boron. This is where return-to-power could occur.

Below is the group input with the presence of the control rod with 'CRD' label.

```
TFU={             }  BOR= {               }  ROD='CRD'  * Large Steam Line Break (RODDED)

TFU={             }  BOR= {   }             ROD='CRD'  * Small Steam Line Break Check (RODDED)

TMO={   }  TFU={           }  BOR= {    } ROD='CRD'  * Small Steam Line Break Check (RODDED)

TMO={   }  TFU={           }   BOR= {   } ROD='CRD'  * Small Steam Line Break Check (RODDED)

TMO={   }  TFU={           }  BOR={             }  ROD='CRD' * Small Steam Line Break
(RODDED)
```

History Effects

The last section of region 9 is the evaluation of history effects that are different than those evaluated explicitly in the case matrix as they relate to accident and post-accident conditions. Three histories are examined: Moderator temperature at inlet and near outlet conditions, boron at nearly double the base and fuel temperature at inlet and average conditions.

From the history depletions, branch cases are run at cold zero power steam line break conditions to evaluate any effects on the potential return to power conditions. The boron conditions are representative of the system that could be already borated or being borated post-accident. This also includes xenon free for maximum reactivity.

```
TTL *MODERATOR TEMPERATURE HISTORY

TMO={          }

DEP  {     }

COE ,, {    }

TMO={   } TFU={   } BOR={    }

XEN={  }PDE={  }TMO={    }TFU={   } BOR={    }


TTL *BORON HISTORY

BOR={    }

DEP  {    }

COE ,, {    }

TMO={   } TFU={   } BOR={    }

XEN={  } PDE={  } TMO={    } TFU={   } BOR={    }


TTL *FUEL TEMPERATURE HISTORY

TFU={       }
```

```
DEP  {      }
COE ,, {    }
TMO={    } TFU={    } BOR={     }
XEN={   }PDE={   }TMO={    } TFU={    } BOR={     }
```

Interpolation and Extrapolation Audit Matrix

The purpose of this audit matrix was to quantify the interpolation (and in a few cases extrapolation) errors from using a sparse case matrix. To accomplish this CASMO5 calculations at the midpoints between the S5C case matrix points are run and compared to the same audit cases in SIMULATE5 using the normal case matrix library.

The midpoints examined are based on the base conditions and those provided in the CASMO5 user manual (Table 2.8) for PWR's without removable burnable absorbers. The variables examined are:

1) Moderator Temperature (TMO)
2) Soluble Boron Concentration (BOR)
3) Fuel Temperature (TFU)
4) The presence of control rods (CRD)
5) Xenon (Xe)
6) Void (VOI)
7) Shut Down Cooling (SDC)
8) History Effects for Fuel and Moderator Temperature at Midpoints

The following sections describe the approach to determining the evaluations point inputs.

Average Moderator Temperature (TMO) Values

The TMO values are calculated using the S5C case matrix description along with the provided base conditions. For this analysis the base condition is assumed to be { } for the TMO value.

The values from the S5C case matrix are as follows:

TMO(K) = { }, **tmo{** }, tmo, **tmo{** }

Where the lower case **tmo** represents the base condition. The resulting points run by S5C would then be:

TMO(K) = { **}**

Resulting in midpoints that are:

TMO(K, Midpoint) = { }

The { } point represents an extrapolation from the S5C values; some nodes at the exit of the core could conceivably approach this temperature.

Average Fuel Temperature (TFU) Values

The TFU values are calculated using the S5C case matrix description along with the provided base conditions. For this analysis the base conditions is assumed to be { } for the TFU value.

The values from the S5C case matrix are as follows:

TFU(K) = TFU= { }, **tmo{** }, { }

Where the lower case **tmo** = { }. The resulting points run by S5C would then be:

TFU(K) = TFU= { }

Resulting in midpoints that are:

TFU(K, Midpoint) = { }

The TFU values used in the analysis were perturbed from the midpoints to values of { } and { }.

Average Soluble Boron Concentration (BOR) Values

The BOR values are calculated using the S5C case matrix description along with the provided base conditions. For this analysis, the base condition is assumed to be { }ppm for the BOR value.

The values from the S5C case matrix are as follows:

BOR(ppm) = { }**, bor, {** }**bor, {** **}**

Where the lower case **bor** = { }ppm the base value. The resulting points run by S5C would then be:

BOR(ppm) = { **}**

Resulting in midpoints that are:

BOR(ppm, Midpoint) = { }

The { } ppm point represents an extrapolation from the S5C values, but some shutdown and post-accident conditions may reach these values.

Average Void Fraction (VOI) Values

The void fraction, VOI, values are calculated using the S5C case matrix description.

The values from the S5C case matrix description are as follows:

VOI(%) ={ } TMO=Tsat

where TSAT is the saturation temperature at the pressure specified in the case. In this case, it is { } bar, with a corresponding TSAT of { }K or about { }. The CASMO5 steam tables when the S5C case matrix is run say that TSAT is { }K. That value is within differences of various steam table interpolations and will be used for this analysis.

The resulting points run by S5C would then be:

VOI(%) = { } TMO={ }K

Resulting in midpoints that are:

VOI(%) = { } TMO={ }K

Shut Down Cooling Time (SDC) Values

The shutdown cooling (SDC) values are calculated using the S5C case matrix description and are:

SDC { }/'Y'

SDC are evaluated at cold zero power conditions resulting in the following midpoints for analysis here:

SDC { } /'Y'

The { } and { } year values extrapolate off the ends of the S5C case matrix.

Evaluating Results

An acceptance criteria was used to determine the adequacy of the results. The limits were a primary reactivity difference limit of { } pcm and a secondary limit of { } pcm. Nearly all points fall within these ranges with a vast majority below the { } pcm threshold.

The results for the PWR operational condition audit matrix show consistent results across all the lattice types with average errors typically well below the { } pcm criteria. Sections where larger errors exist are in the { } at off normal conditions. Other sections where xenon free conditions are modeled exhibit { } errors in general since the base depletion conditions of the case matrix are with equilibrium xenon. A representative plot from the analysis is shown in Figure 1 for a WH 17x17 lattice with average errors shown in Table 1.

The results for the PWR interpolation audit matrix show consistent results across all the lattice types with average errors typically well below the { } pcm criteria. Like the operational audit comparisons, the { } errors are attributed to off normal and { } conditions along with rodded { } conditions. Similar behavior was also observed for xenon free conditions. A representative plot from the analysis is shown in Figure 2 for a WH 17x17 lattice that includes IFBA-coated fuel with the average errors shown in Table 2.

The results of the analysis demonstrate that the accuracy of the cross-section library generated by the S5C case matrix in CMS5 is sufficient for analyzing PWR reactor cores.

Table 1: WH17x17 No BP Operational Audit Average Errors

Section	Absolute Average Error		Conditions	SP #
1	{ }	pcm	At Power ARO Cases + Nonphysical	1-1590
2	{ }	pcm	At Power Rodded Cases + Nonphysical	1591-3181
3	{ }	pcm	AT Power SDC	3182-3482
4	{ }	pcm	Isothermal at Power with Xenon	3483-4514
5	{ }	pcm	Isothermal at Power Rodded with Xenon	4515-5589
6	{ }	pcm	Isothermal ARO No Xenon	5590-6621
7	{ }	pcm	Isothermal Rodded No Xenon	6622-7696
8	{ }	pcm	Isothermal SDC	7697-9278
9	{ }	pcm	Off Normal History Conditions and Accident Conditions	9279-10854

Figure 1: WH 17x17 Lattice No BP with AIC RCCA Audit Results

Table 2: WH17x17 IFBA Interpolation Audit Average Errors

Section	Absolute Average Error		Conditions	SP #
1	{ }	pcm	TMO + TFU	1-1332
2	{ }	pcm	TMO + TFU No Xe	1333-2622
3	{ }	pcm	BOR + TMO	2623-3653
4	{ }	pcm	BOR + TMO No Xe	3654-4686
5	{ }	pcm	TMO+CRD	4687-4944
6	{ }	pcm	TMO+CRD No Xe	4945-5202
7	{ }	pcm	BOR + VOI	5203-5891
8	{ }	pcm	BOR+VOI NO Xe	5892-6578
9	{ }	pcm	CRD+VOI	6579-6750
10	{ }	pcm	CRD+VOI No Xe	6751-6922
11	{ }	pcm	SIM3 SDC	6923-7395
12	{ }	pcm	TMO, TFU and BOR History	7396-7647

Figure 2: WH17x17 IFBA Interpolation Audit Error

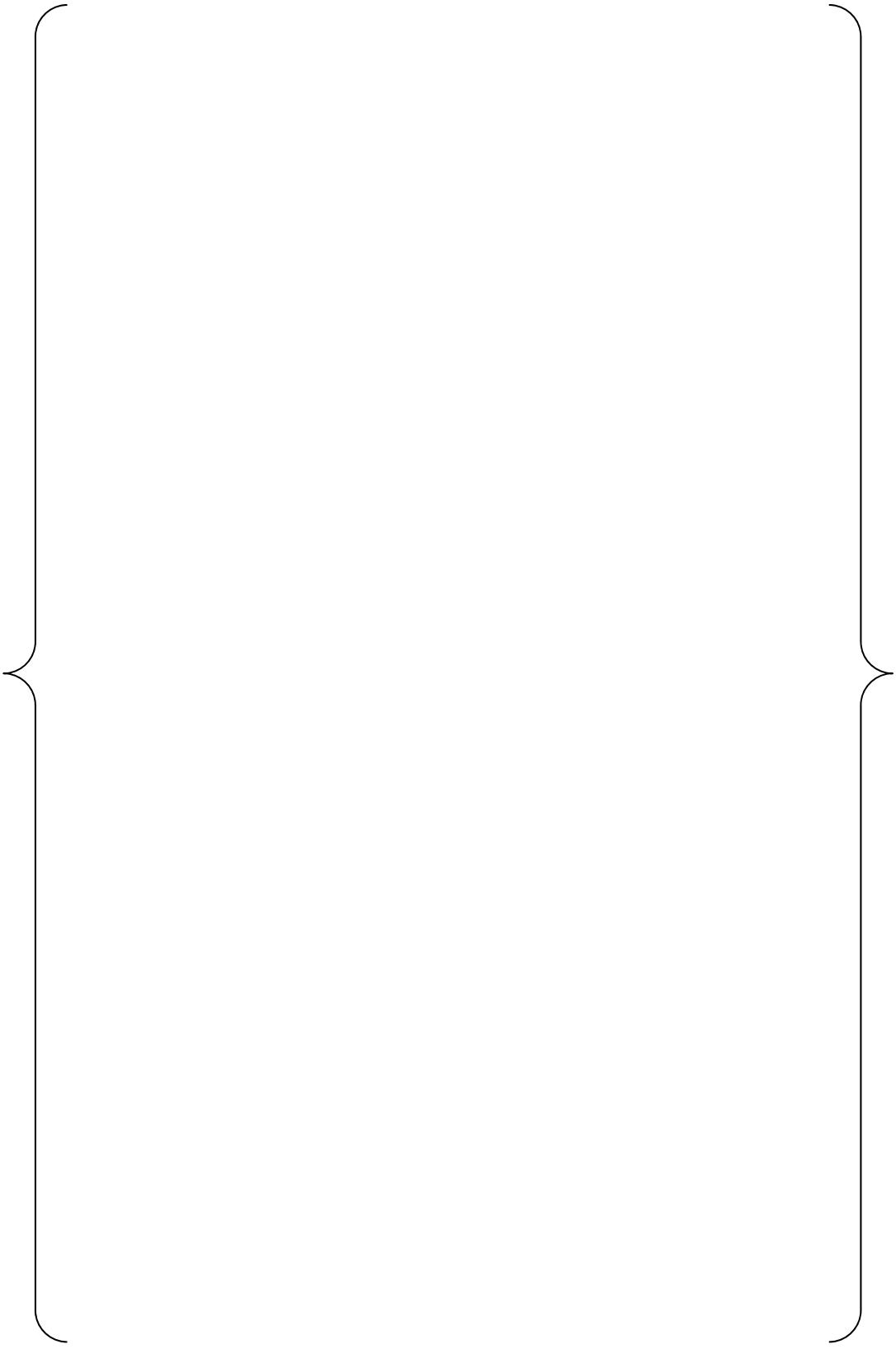

References:

1. B. Haugh, "S5C Case Matrix Assessment", SSP-14-P01/020-C, 2015.

c. Modeling of the KRITZ3 Experiments in CASMO5

The KRITZ-3 high temperature critical experiments described in Reference 1, were performed under contract between Kraftwerk Union Aktiengesellschaft Mülheim West Germany (KWU) and AB Atomenergi Studvik Sweden. These experiments have been modeled in CASMO5 (Reference 2) to benchmark the code against measured data.

The critical experiments are unique in that they are not only at cold (i.e., room temperature) conditions. The temperature range is from { } to { }. While this range does not cover all operational conditions of a PWR, it shows the ability of CASMO5 to predict reactivity as function of varying operational conditions.

The experimental geometry is a cylindrical core loaded with three different fuel pins, Uranium fuel enriched to { } w/o ^{235}U and mixed oxide fuel with a Plutonium fissile content of { } and { } w/o respectively. The Plutonium fuel pins, when present in the core, were loaded in the central zone. Eight different core configurations have been analyzed with different critical conditions such as variation in; boron concentration, moderator temperature, water level/neutron leakage (axial buckling) and with or without presence of control rod fingers. The eight core configurations, summarized in Table 1, are divided in two subsets of layout; small (see Figure 1) or large (see Figure 2) water holes depending on CR finger cluster studied.

The 89 configurations were modeled in CASMO5 and show good agreement to measured data. The summary of the eigenvalue results is presented in Table 2. Of the 89 cases, 5 of the experiments contained detailed normalized fission rate measurement data. These were also compared with CASMO5 predictions. Figure 4 through Figure 8 show the distributions of the measurements collapsed to the upper right quarter core, as done in Reference 1. These comparisons include the CASMO5 predicted fission rate, measured fission rate and absolute percent difference. Table 3 summarizes the fission rate comparison results and shows CASMO5 results agree well with the measurements.

These critical experiments covered a wide range of operating temperatures to better demonstrate code performance at closer to PWR operating conditions. The calculated CASMO5 eigenvalues are plotted as a function of temperature in Figure 3 with good results. As can be seen in the figure there is a slight trend in eigenvalue with temperature, an approximate increase of { } pcm of the average. This trend is within the minimum to maximum spread of data, roughly { } pcm.

Overall the CASMO5 results compare well with measured reactivity and fission rate data. This shows that CASMO5 can perform PWR calculations at varying operating temperatures.

Table 1: KRITZ-3 Core Configuration Summary

Core Type	Fuel	Water holes	Control rods	Acronym
1	All UO2	Small	-	U-WH1
1	All UO2	Small	16	U-CR1
1	Central Pu	Small	-	Pu-WH1
1	Central Pu	Small	16	Pu-CR1
2	All UO2	Large	-	U-WH2
2	All UO2	Large	5	U-CR2
2	Central Pu	Large	-	Pu-WH2
2	Central Pu	Large	5	Pu-CR2

Figure 1: KRITZ-3 Small Water Hole Model Geometry (U-WH1)
(Copied from Reference 1)

Figure 2: KRITZ-3 Large Water Hole Model Geometry (U-WH2)
(Copied from Reference 1)

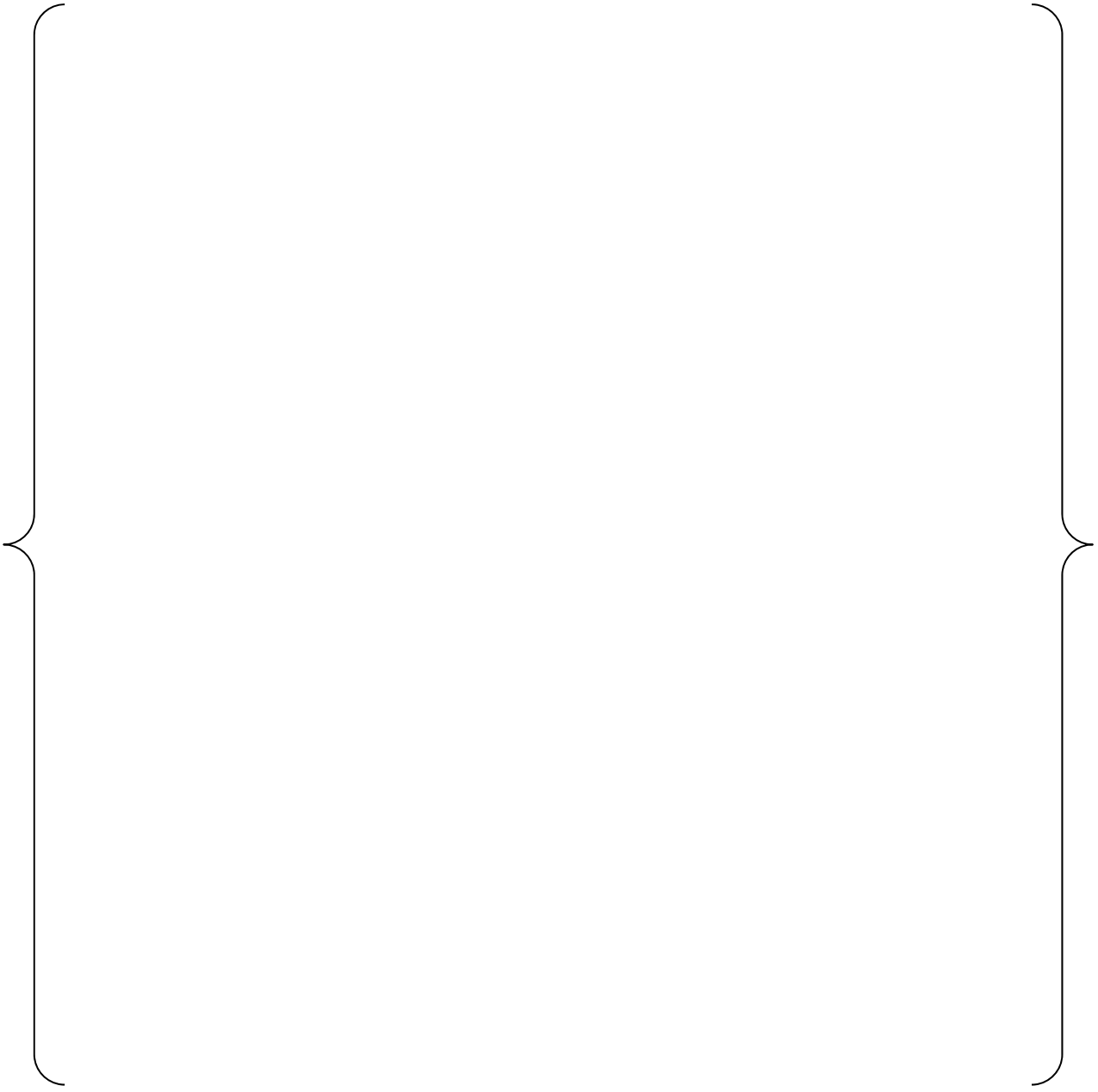

Table 2: KRITZ-3 CASMO5 Summary Eigenvalue Results

Core type	Average Eigenvalue	Standard-Deviation of Differences (pcm)	Number of measurement points -
All	{ }	{ }	89
UO2	{ }	{ }	43
Pu	{ }	{ }	46
Type 1 Small Guide Tubes			
UO_2 and Pu core	{ }	{ }	45
AIC CR inserted	{ }	{ }	23
Type 2 Big Guide Tubes			
UO2 and Pu core	{ }	{ }	44
B_4C CR inserted	{ }	{ }	20

Figure 3: KRITZ-3 CASMO5 Eigenvalue vs. Temperature

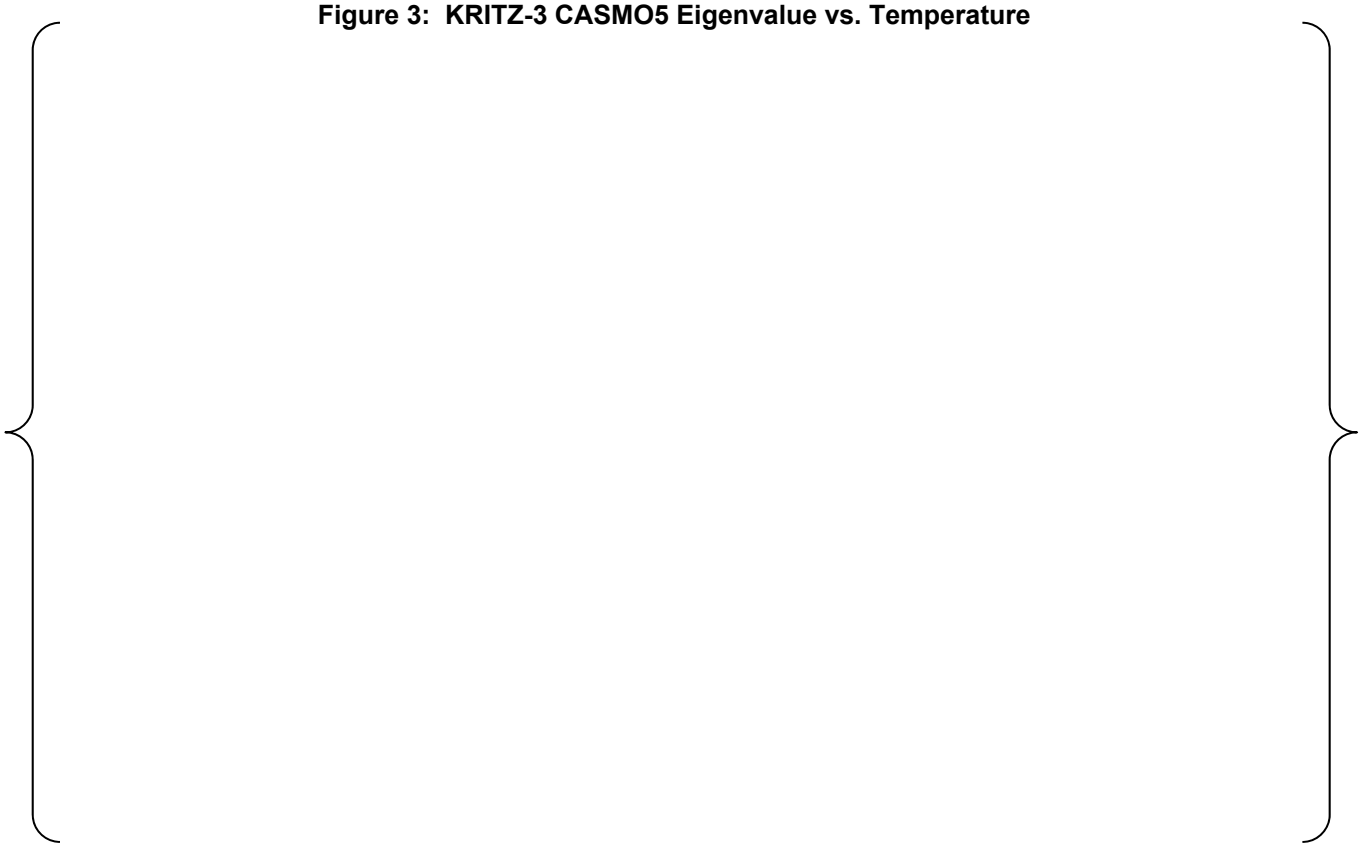

Figure 4: KRITZ-3 U-WH1 Fission Rate Comparison Map { }

Figure 5: KRITZ-3 Pu-WH1 Fission Rate Comparison Map{ }

Figure 6: KRITZ-3 U-WH2 Fission Rate Comparison Map { }

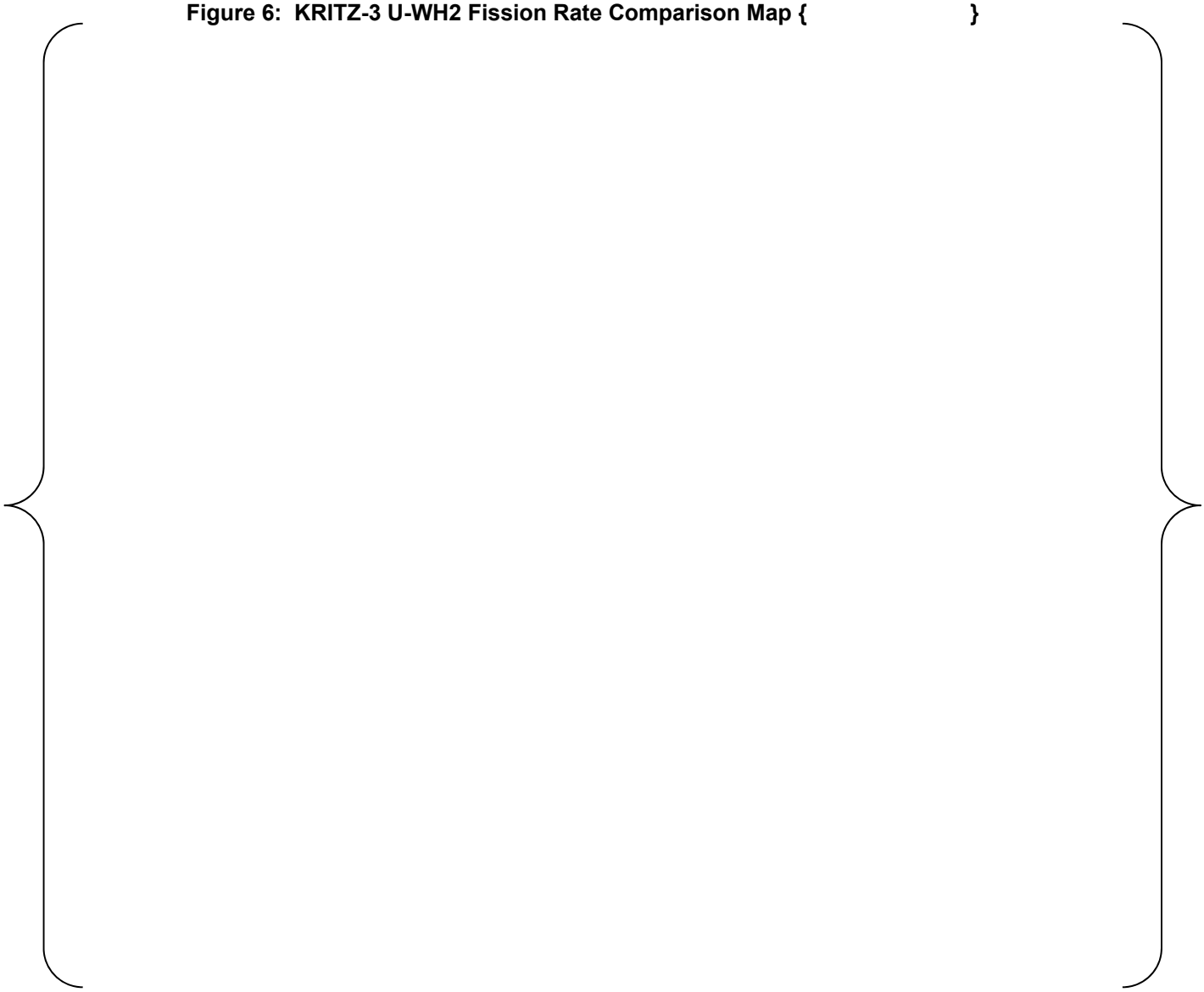

Figure 7: KRITZ-3 Pu-WH2 Fission Rate Comparison Map { }

Figure 8: KRITZ-3 Pu-WH2 Fission Rate Comparison Map { }

Table 3: KRITZ-3 CASMO5 Fission Rate Summary Results

Core Type	Value	Number of Measured Points
All Cores		
Average Absolute Error	{ }	110
Absolute Error Standard Deviation	{ }	
UO_2 Cores		
Average Absolute Error	{ }	31
Absolute Error Standard Deviation	{ }	
Pu Cores		
Average Absolute Error	{ }	79
Absolute Error Standard Deviation	{ }	

References:

1. E. Johansson *et al.*,"KRITZ-3 Experiments", Internal Report, AB Atomenergi, Studsvik, Sweden, 1973.

2. M. Kruners, “Modeling of the KRITZ-3 Critical Experiment in CASMO5, “ SSP-14-P01/002-C, 2014

d. TCA Reflector Critical Experiment Analysis in CASMO5

The TCA experiment was chosen to demonstrate that CASMO5 can appropriately model reflectors of varying thickness, and predict kinetic data as compared to measurement.

Experimental critical configurations were reported for 2.6% enriched typical 15x15 PWR fuel assemblies with various configurations of steel and steel/water reflector slabs in Reference 1. The experiments were carried out using the Tank type Critical Assembly (TCA) at Tokai Research Establishment of JAERI. The objectives were to measure the reactivity effect of the steel reflector plates and reflectors containing about 90% steel and 10% water. A diagram of the experiment configuration is shown in Figure 1.

Figure 1: TCA Reflector Experiment Configuration
(Copied from Reference 1)

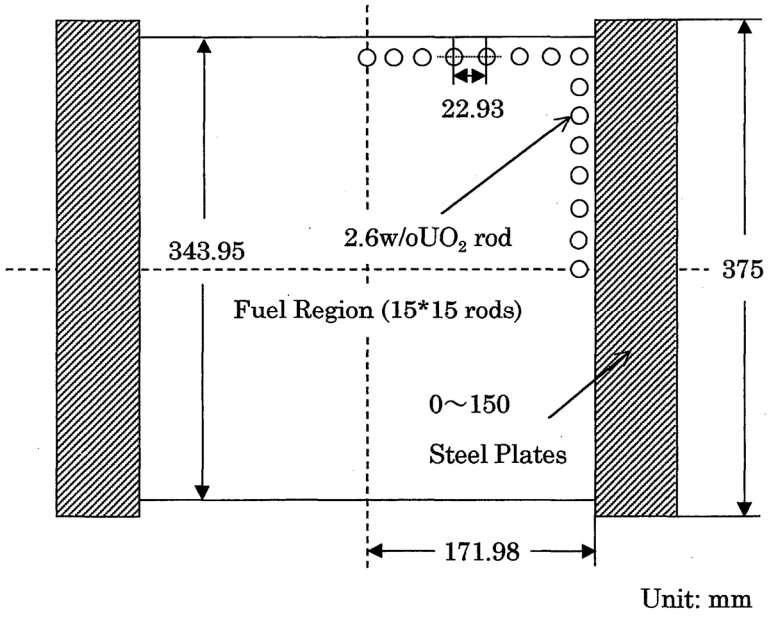

The reported experimental conditions and results allow for benchmark comparisons of the reported reflector reactivity worth, and each critical configuration's calculated eigenvalue to CASMO5 (Reference 2) results under the same conditions. In addition, the CASMO5 calculated β_{eff}/l^* for a bare water reflected configuration is compared.

The eigenvalue results calculated in CASMO5 are shown below in Table 1. In general the results compare well, although there {is a small increasing trend of eigenvalue} with increasing steel reflector thickness.

The comparison of the ratio of β_{eff}/l^* in Table 2 shows very good agreement with the measurement and is within the experimental uncertainty.

The reactivity effect of the different reflector configurations is compared in Table 3. The results of CASMO5 compare well with the benchmark and show very similar trends as can been seen in Figure 2 and Figure 3.

The overall results show that CASMO5 can appropriately model heavy reflectors. Also the kinetics data measurements show that the information used in CASMO5 is appropriate for PWR modeling.

Table 1: CASMO5 TCA Eigenvalue and β_{eff} Results

Reflector Configuration	CASMO5 B_{eff}	CASMO5 Eigenvalue	Delta (pcm) from Unity
0.0 cm steel	{ }	{ }	{ }
0.56 cm steel	{ }	{ }	{ }
2.80 cm steel	{ }	{ }	{ }
3.36 cm steel	{ }	{ }	{ }
6.16 cm steel	{ }	{ }	{ }
8.96 cm steel	{ }	{ }	{ }
11.76 cm steel	{ }	{ }	{ }
15.12 cm steel	{ }	{ }	{ }
3.73 cm steel/water	{ }	{ }	{ }
6.79 cm steel/water	{ }	{ }	{ }
9.96 cm steel/water	{ }	{ }	{ }
13.07cm steel/water	{ }	{ }	{ }
15.66 cm steel/water	{ }	{ }	{ }

Table 0-10: CASMO5 TCA β_{eff}/l^* Comparison (Bare Water Reflected)

	CASMO5	Measured
β_{eff}/l^*	{ }	{ }

Table 2: CASMO5 TCA Reflector Reactivity Comparisons

Reflector Configuration	"Reactivity Effect" CASMO5 (%Δk/k)	"Reactivity Effect" Reported (%Δk/k)	"Reactivity Effect" Percent Difference
0.0 cm steel	N/A	0.000	N/A
0.56 cm steel	{ }	{ }	{ }
2.80 cm steel	{ }	{ }	{ }
3.36 cm steel	{ }	{ }	{ }
6.16 cm steel	{ }	{ }	{ }
8.96 cm steel	{ }	{ }	{ }
11.76 cm steel	{ }	{ }	{ }
15.12 cm steel	{ }	{ }	{ }
3.73 cm steel/water	{ }	{ }	{ }
6.79 cm steel/water	{ }	{ }	{ }
9.96 cm steel/water	{ }	{ }	{ }
13.07 cm steel/water	{ }	{ }	{ }
15.66 cm steel/water	{ }	{ }	{ }

Figure 2: TCA Critical Steel Reflector Reactivity Effect

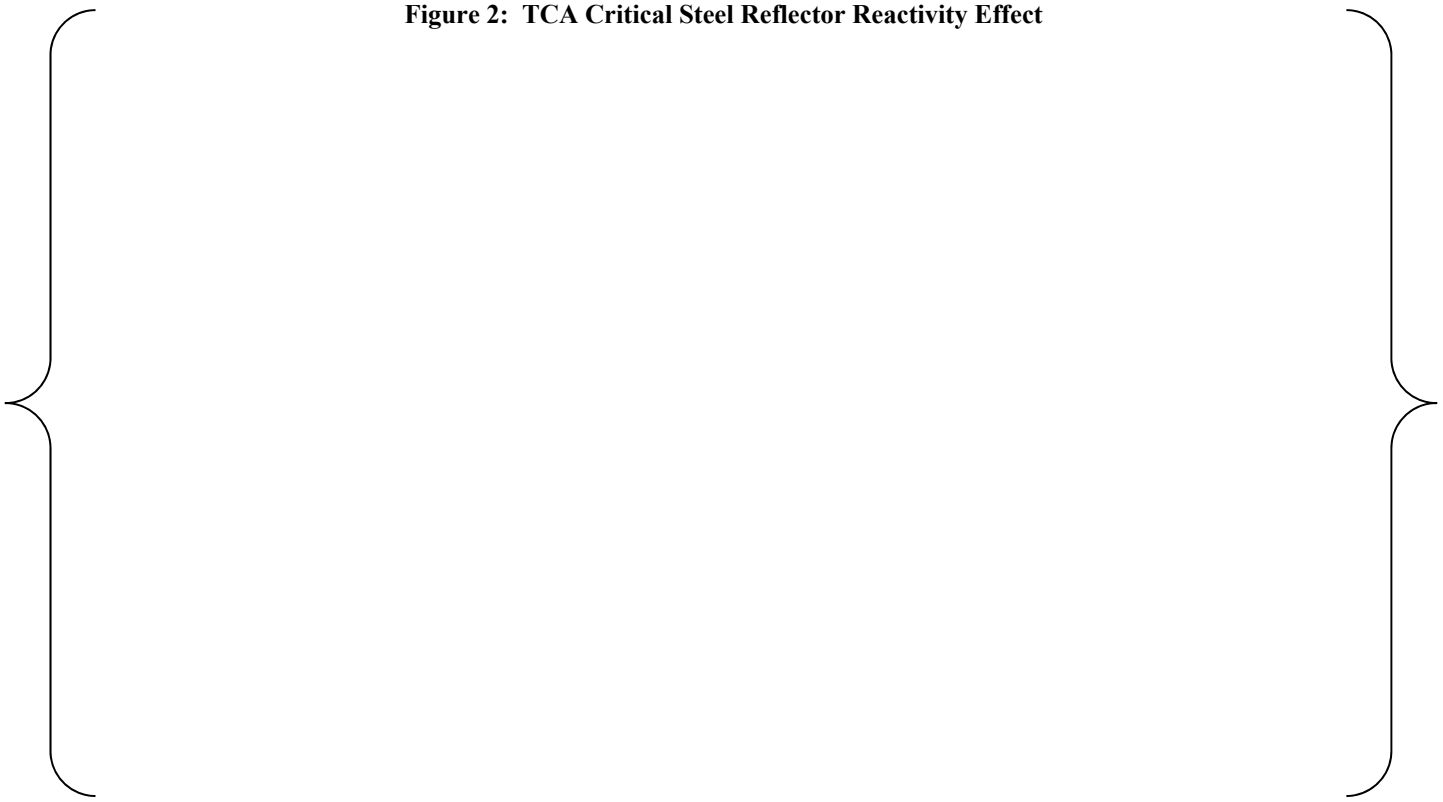

Figure 3: TCA Critical Steel/Water Reflector Reactivity Effect

References:

1. Y Tahara *et al.*, "Reactivity Effect of Iron Reflector in LWR Cores", *Nuclear Science and Technology*, Vol. 28, No.2, p. 102-111.

2. S. Vanevenhoven, “TCA Reflector Critical Experiment Analysis in CASMO5,” SSP-14-P01/005-C, 2014.

e. MCNP6 Lattice Reactivity Comparisons to CASMO5

Comparison calculations have been made between CASMO5 and MCNP6 (Reference 1) to examine the reactivity effects of different operating conditions. These include Doppler temperature defects, moderator temperature defects, soluble boron worth and control rod worth. The calculations span a wide range of PWR lattice designs and conditions as listed below.

- Lattice Designs: 14x14, 15x15, 17x17, 14x14 CE
- Boron concentrations (ppm): 0 - 2500
- Fuel enrichment (wt% U-235): 2.5 - 5.0
- Moderator temperature (F): 70 - 620
- Fuel temperature (K): 293 - 1200
- Removable / Discrete BP type: PYREX, WABA, Discrete B_4C (CE)
- Integral BP Gadolinia (wt% Gd): 2.0 - 8.0
- Integral BP IFBA (ZrB_2) (mg/cm B10): 1.5 - 3.0
- Control rod absorber type: AIC, B_4C, HAF, W

The analysis is performed to augment the measured data compared earlier. Given that experimental data is not available over the range of conditions listed above, the use of Monte-Carlo and continuous energy cross-sections is the next best reference.

The two codes are compared with consistent nuclear data (i.e. ENDF/B-VII-R1) to provide insight into any significant modeling differences. The results are presented in Table 1 through Table 4 and show reasonable agreement between CASMO5 and MCNP6.

A small negative bias in the reactivity worth of most absorber types is observed, which indicates the MCNP6 worth is slightly higher at the fresh fuel conditions analyzed. The Moderator Temperature and Doppler defects are compared in Figure 1 and Figure 2 respectively and show little trend. No other trends were noted with other variables.

The lattice reactivity comparisons with MCNP6 show there are no large systematic biases that need to be addressed before providing the CASMO5 data to SIMULATE5.

Additional comparisons for IFBA are presented since there is an absence of obtainable critical experiment data to validate against. The comparisons between CASMO5 to MCNP6 are used to show

that CASMO5 calculations that contain IFBA perform as well as other materials. These include the single assembly comparisons of the total fission rate on a normalized basis. The comparisons for two 15x15 lattice designs at hot conditions are shown in Figure 3 and Figure 4. The comparisons for two 17x17 lattice designs at hot conditions are shown in Figure 5 and Figure 6. The figures show the SE symmetric octant of the lattice. A summary of the results using all pins in the lattice is shown in Table 5 and shows excellent agreement between CASMO5 and MCNP6.

Table 1: CASMO5 BOL Reactivity Benchmark vs. MCNP6, Global Perturbations

Parameter	Lattice Configuration	Average Relative Error (%)	Std. Deviation of Relative Error (%)	Number of Observations
Soluble Boron Worth	17x17	{ }	{ }	60
	15x15	{ }	{ }	60
	14x14 (W)	{ }	{ }	60
	14x14 (CE)	{ }	{ }	60
Moderator Temp. Defect	17x17	{ }	{ }	6
	15x15	{ }	{ }	6
	14x14 (W)	{ }	{ }	6
	14x14 (CE)	{ }	{ }	5
Fuel Temperature (Doppler) Defect	17x17	{ }	{ }	6
	15x15	{ }	{ }	6
	14x14 (W)	{ }	{ }	6
	14x14 (CE)	{ }	{ }	6

Table 2: CASMO5 BOL Reactivity Benchmark vs. MCNP6, Control Rod Worth

Parameter	Lattice Configuration	Average Relative Error (%)	Std. Deviation of Relative Error (%)	Number of Observations
AIC Control Rods	17x17	{ }	{ }	3
	15x15	{ }	{ }	3
	14x14 (W)	{ }	{ }	3
	14x14 (CE)	{ }	{ }	3
B4C Control Rods	17x17	{ }	{ }	3
	14x14 (CE)	{ }	{ }	3
Hafnium Rods	17x17	{ }	{ }	3
Tungsten Control Rods	17x17	{ }	{ }	3

Table 3: CASMO5 BOL Reactivity Benchmark vs. MCNP6, Integral Absorbers

Parameter	Lattice Configuration	Average Relative Error (%)	Std. Deviation of Relative Error (%)	Number of Observations
IFBA @ 1.5 mg/cm	17x17 (16 Rods)	{ }	{ }	3
	17x17 (264 Rods)	{ }	{ }	3
	15x15 (16 Rods)	{ }	{ }	3
	15x15 (148 Rods)	{ }	{ }	3
	14x14 (16 Rods)	{ }	{ }	3
	14x14 (120 Rods)	{ }	{ }	3
IFBA @ 3.0 mg/cm	17x17 (16 Rods)	{ }	{ }	3
	17x17 (264 Rods)	{ }	{ }	3
	15x15 (16 Rods)	{ }	{ }	3
	15x15 (148 Rods)	{ }	{ }	3
	14x14 (16 Rods)	{ }	{ }	3
	14x14 (120 Rods)	{ }	{ }	3
2.0 w/o Gadolinium	17x17 (4 Rods)	{ }	{ }	3
	17x17 (16 Rods)	{ }	{ }	3
	15x15 (4 Rods)	{ }	{ }	3
	15x15 (16 Rods)	{ }	{ }	3
	14x14 (4 Rods)	{ }	{ }	3
	14x14 (12 Rods)	{ }	{ }	3
	14x14 (CE) (4 Rods)	{ }	{ }	3
	14x14 (CE) (16 Rods)	{ }	{ }	3
8.0 w/o Gadolinium	17x17 (4 Rods)	{ }	{ }	3
	17x17 (16 Rods)	{ }	{ }	3
	15x15 (4 Rods)	{ }	{ }	3
	15x15 (16 Rods)	{ }	{ }	3
	14x14 (4 Rods)	{ }	{ }	3
	14x14 (12 Rods)	{ }	{ }	3
	14x14 (CE) (4 Rods)	{ }	{ }	3
	14x14 (CE) (16 Rods)	{ }	{ }	3

Table 4: CASMO5 BOL Reactivity Benchmark vs. MCNP6, Discrete Absorbers

Parameter	Lattice Configuration	Average Relative Error (%)	Std. Deviation of Relative Error (%)	Number of Observations
Removable Discrete BP Rods (Pyrex)	17x17 (4 Rods)	{ }	{ }	3
	17x17 (24 Rods)	{ }	{ }	3
	15x15 (4 Rods)	{ }	{ }	3
	15x15 (20 Rods)	{ }	{ }	3
	14x14 (4 Rods)	{ }	{ }	3
	14x14 (16 Rods)	{ }	{ }	3
Removable Discrete BP Rods (Wet Annular Burnable Absorber)	17x17 (4 Rods)	{ }	{ }	3
	17x17 (24 Rods)	{ }	{ }	3
	15x15 (4 Rods)	{ }	{ }	3
	15x15 (20 Rods)	{ }	{ }	3
Fixed Discrete Burnable Absorber (B4C)	14x14 (CE) (4 Rods)	{ }	{ }	3
	14x14 (CE) (16 Rods)	{ }	{ }	3

Figure 1: CASMO5 vs. MCNP6 Moderator Temperature Defect

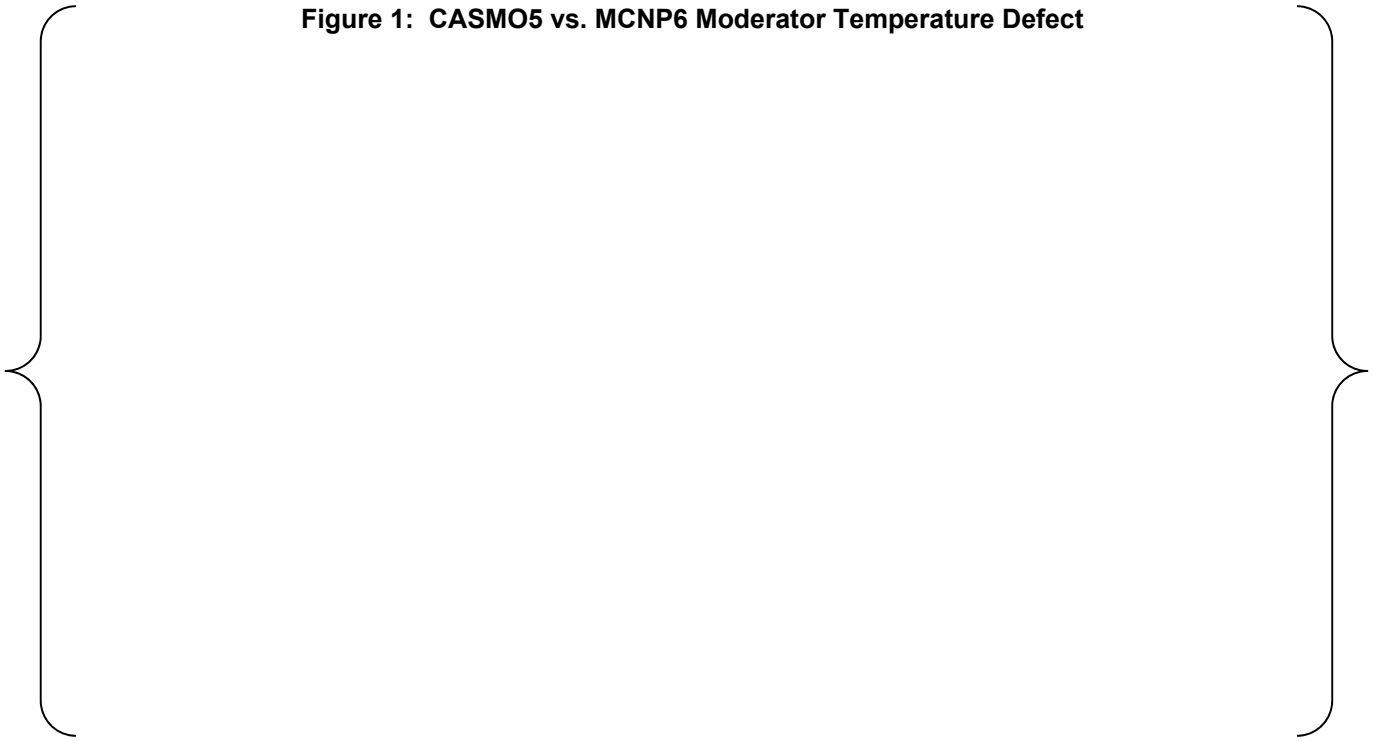

Figure 2: CASMO5 vs. MCNP6 Doppler Defect

Figure 3: W15x15 Hot Fission Rate Comparison, 16 IFBA @ 3.0 mg/cm ^{10}B

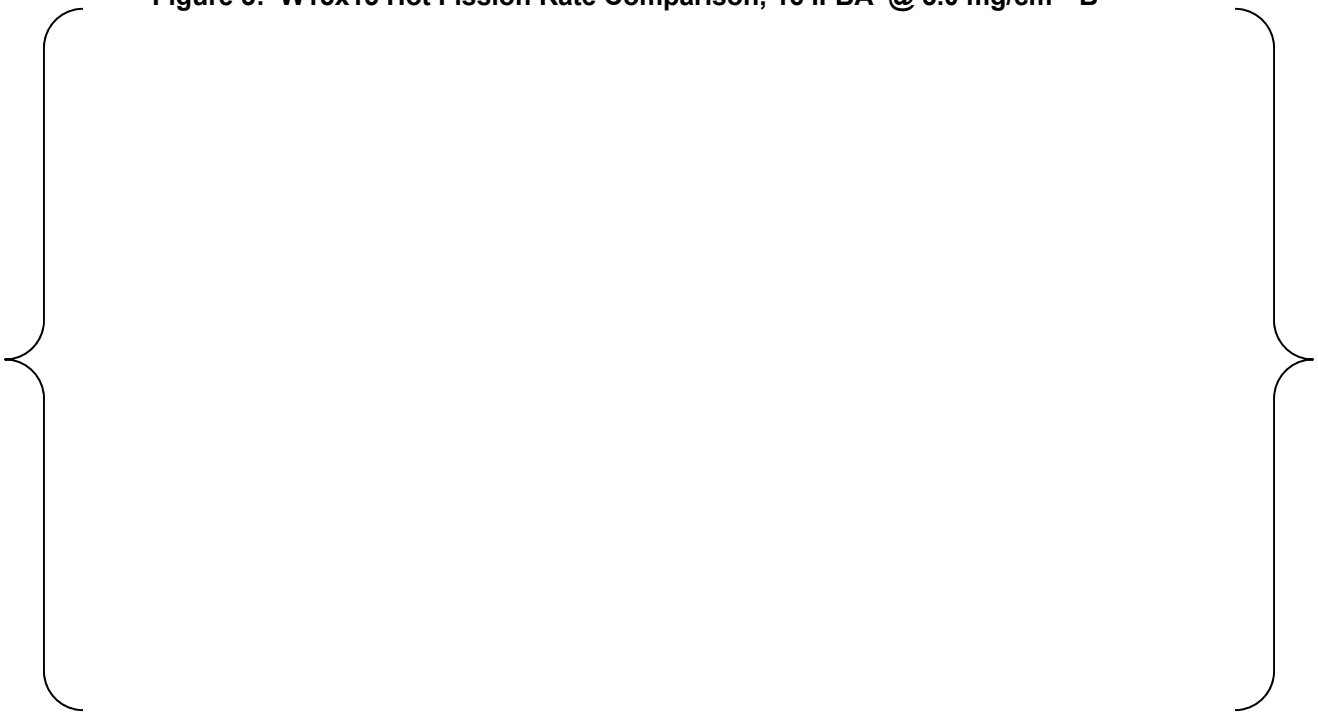

Figure 4: W15x15 Hot Fission Rate Comparison, 148 IFBA @ 3.0 mg/cm ^{10}B

Figure 5: W17x17 Hot Fission Rate Comparison, 16 IFBA @ 3.0 mg/cm ^{10}B

Figure 6: W17x17 Hot Fission Rate Comparison, 264 IFBA @ 3.0 mg/cm ^{10}B

Table 5: IFBA Fission Rate Comparison Summary

Lattice Type	Value	Number of Points
All Lattice, All Pins		
Average Absolute Error	{ }	936
Absolute Error Standard Deviation	{ }	
15x15 Lattice, All Pins		
Average Absolute Error	{ }	408
Absolute Error Standard Deviation	{ }	
17x17 Lattice, All Pins		
Average Absolute Error	{ }	528
Absolute Error Standard Deviation	{ }	
All Lattice, IFBA Pins		
Average Absolute Error	{ }	444
Absolute Error Standard Deviation	{ }	
15x15 Lattice, IFBA Pins		
Average Absolute Error	{ }	164
Absolute Error Standard Deviation	{ }	
17x17 Lattice, IFBA Pins		
Average Absolute Error	{ }	280
Absolute Error Standard Deviation	{ }	

References:

1. E. Wehlage, “MCNP6 Lattice Reactivity Comparison to CASMO5,” SSP-14-P01/009-C, 2014.

23. Provide a copy of the following reference:

N. M. Razali, Y. B. Wah, “Power comparisons of Shapiro-Wilk, Kolmogorov, Lilliefors and Anderson-Darling tests,” Journal of Statistical Modeling and Analytics, Vol 2, No. 1, 21-33, 2011

A copy of the above reference has been submitted along with the RAI responses into the electronic submittal system.